
Geometry of Similarity Comparisons

Puoya Tabaghi

Coordinated Science Lab
ECE Department, UIUC
tabaghi2@illinois.edu

Jianhao Peng

Coordinated Science Lab
ECE Department, UIUC
jianhao2@illinois.edu

Olgica Milenkovic

Coordinated Science Lab
ECE Department, UIUC
milencov@illinois.edu

Ivan Dokmanić

Department of Mathematics and Computer Science
University of Basel
ivan.dokmanic@unibas.ch

Abstract

Many data analysis problems can be cast as distance geometry problems in *space forms* – Euclidean, spherical, or hyperbolic spaces. Often, absolute distance measurements are often unreliable or simply unavailable and only proxies to absolute distances in the form of similarities are available. Hence we ask the following: Given only *comparisons* of similarities amongst a set of entities, what can be said about the geometry of the underlying space form? To study this question, we introduce the notions of the *ordinal capacity* of a target space form and *ordinal spread* of the similarity measurements. The latter is an indicator of complex patterns in the measurements, while the former quantifies the capacity of a space form to accommodate a set of measurements with a specific ordinal spread profile. We prove that the ordinal capacity of a space form is related to its dimension and the sign of its curvature. This leads to a lower bound on the Euclidean and spherical embedding dimension of what we term similarity graphs. More importantly, we show that the statistical behavior of the ordinal spread random variables defined on a similarity graph can be used to identify its underlying space form. We support our theoretical claims with experiments on weighted trees, single-cell RNA expression data and spherical cartographic measurements.

1 Introduction

Distances reveal the geometry of their underlying space. They are at the core of many machine learning algorithms. In particular, finding a geometrical representation for point sets based on pairwise distances is the subject of distance geometry problems (DGPs). Euclidean DGPs have a rich history of applications in robotics [1, 2], wireless sensor networks [3], molecular conformation analysis [4] and dimensionality reduction [5]. One is typically concerned with finding a geometric representation for a set of measured Euclidean distances [6]. Beyond Euclidean DGPs, recent works have focused on hyperbolic geometry methods in data analysis, most notably when dealing with hierarchical data. Social and FoodWeb networks [7, 8], gene ontologies [9], and Hearst graphs of hypernyms [10] are interesting examples of hierarchical datasets. Spherical embeddings represent sets of points on a (hyper)sphere [11], and have found applications in astronomy [12], distance problems on Earth [13], and texture mapping [14]. Euclidean, spherical and hyperbolic geometries are categorical examples of constant curvature spaces, or space forms, which are characterized by their curvature and dimension. The above examples represent instances of metric embeddings in space forms, as opposed to what is termed *nonmetric embeddings*. In the latter setting, one is provided with nonmetric information about data points, such as quantized distances or ordinal measurements such as comparisons or rankings.

We argue that nonmetric information such as *distance comparisons* carries valuable information about the space the data points originated from. To formally state our claims, assume that we are given a set of points x_1, \dots, x_N in an unknown metric space S . In nonmetric embedding problems [15, 16], we work with dissimilarity (similarity) measurements of the form

$$\forall m, n \in [N] \stackrel{\text{def}}{=} \{1, \dots, N\} : y_{m,n} = \phi(d(x_m, x_n)),$$

where $d(x_m, x_n)$ is the distance between x_m and x_n in S , and $\phi(\cdot)$ is an unknown monotonically increasing (or decreasing) function. Since ϕ is unknown, we can *only* interpret the measurements as distance comparisons or ordinal measurements, i.e., if the entities indexed by n_1, n_2 are more similar than those indexed by n_3, n_4 , then

$$y_{n_1, n_2} \leq y_{n_3, n_4} \xleftrightarrow{\text{increasing } \phi} d(x_{n_1}, x_{n_2}) \leq d(x_{n_3}, x_{n_4}).$$

We hence ask: *What do distance/similarity comparisons as those described above reveal about the space S ?* Our work shows, for the first time, that one can use ordinal measurements to deduce the sign of the curvature and a lower-bound for the dimension of the underlying space form (in Euclidean and spherical spaces). The main results of our analysis are as follows.

1. We introduce the notion of *ordinal spread* of the sorted distance list, which is of fundamental importance in the study of the geometry of distance comparisons. The spread of ordinal measurements describes a pattern in which entities appear in the sorted list of distances, i.e., the ordinal spread gives the ranking of the first appearance of a data point in the list. This notion is related to another important geometric entity termed the *ordinal capacity*.
2. We define the notion of *ordinal capacity* of a space form to characterize the space’s ability to host extreme patterns of ordinal spreads (computed from similarity measurements). We show that the ordinal capacity of a space form is related to its dimension and curvature sign. The ordinal capacity of Euclidean and spherical spaces are equal and grow exponentially with their dimensions, while the ordinal capacity of a hyperbolic space is infinite for any possible dimension of the space.
3. We derive a deterministic lower bound for Euclidean and spherical embedding dimensions using ordinal spreads and the (finite) ordinal capacity. We also associate an *ordinal spread random variable* with (1) a set of random points in a space form, and (2) a set of random vertex subsets from a similarity graph – a complete graph with edge weights corresponding to similarity scores of their defining nodes. The distributions of these random variables serves as a practical tool to identify the underlying space form given a similarity graph.
4. We illustrate the utility of our theoretical analysis by using them to correctly uncover the hyperbolicity of weighted trees. Moreover, we use them to detect Euclidean and spherical geometries for ordinal measurements derived from local and global cartographic data. Finally, we use the ordinal spread variables to determine the degree of heterogeneity of cell populations based on noisy scRNAseq data and how data imputation influences the geometry of the cell space trajectories.

Due to space limitations, all proofs, algorithms, and extended discussions are delegated to the Supplement.

1.1 Related Works

In many applications we seek a representation for a group of entities based on their distances, but the exact magnitudes of the distances may be unavailable. What often *is* available (and prevalent) in applied sciences are nonmetric – dissimilarity or similarity – measurements: In neural coding [17], developmental biology [18], learning from perceptual data [19], and cognitive psychology [20]. Unfortunately, the datasets used in most of these studies are small (often involving less than 100 entities) and have limited utility for learning tasks that require sufficiently large sample complexity.

Nonmetric embedding problems date back to the works of Shepard [21, 22] and Kruskal [15]. Inspired by the Shepard-Kruskal scaling problem, Agarwal *et al.* [16] introduce generalized nonmetric multi-dimensional scaling, a semidefinite relaxation used to embed dissimilarity (or similarity) ratings of a set of entities in Euclidean space. Stochastic triplet embeddings [23] and crowd kernel learning [24] are used to embed triadic comparisons using probabilistic information. Tabaghi *et al.* [25] propose a semidefinite relaxation for metric and nonmetric embedding problems in hyperbolic space. In all

these scenarios, the embedding space has to properly represent the measured data. For example, in developmental biology and cancer genomics, single-cell RNA sequencing (scRNAseq) is used to differentiate cell types and cycles. The classification results have important implications for lineage identification and monitoring cell trajectories and dynamic cellular processes [26]. Klimovskaia *et al.* [18] use hyperbolic rather than Euclidean spaces for low-distortion embedding of complex cell trajectories (hierarchical structures).

Learning from distance comparisons is an active area of research. Among the relevant research topics are ranking objects from pairwise comparisons [27, 28], theoretical analysis of necessary number of distance comparisons to uniquely determine the embedding [29], nearest neighbor search [30], random forests [31], and classification based on triplet comparisons [32]. Understanding the underlying geometry of ordinal measurements is important in designing relevant algorithms.

Related to nonmetric embedding problems are the various techniques that study topological properties of point clouds independently of the choice of metric and of the geometric properties such as curvature [33]. An important problem in this domain is to detect intrinsic structure in neural firing patterns, invariant under nonlinear monotone transformations of measurements. Giusti *et al.* [17] propose a method based on clique topology of the graph of correlations between pairs of neurons. The clique topology of a weighted graph describes the behavior of cycles in its order complex [17] as a function of edge densities; these entities are also known as *Betti curves*. The statistical behavior of Betti curves is used to distinguish random and geometric structures of moderate sizes in Euclidean space. The more recent work of Zhou *et al.* [34] generalizes this statistical approach to hyperbolic spaces. These two works are the most closely related contributions to our proposed problem area. Nevertheless, the technical approaches used in there and in our work are fundamentally different. First, we provide a theoretical foundation for the study of geometric properties of space forms using similarity comparisons and derive the first known rigorous results related to their dimensions and curvatures. Second, we propose a computationally efficient method for inferring the sign of the curvature. The proposed statistical method can operate on large datasets as it uses subsampling techniques. Furthermore, we introduce new application areas in outlier identification, heterogeneity detection and imputation analysis for single-cell data measurements. To the best of our knowledge, we report the first study regarding the effect of different imputation degrees on the geometry of similarity measurements in these datasets.

2 The Ordinal Spread

Preliminaries. A space form is a complete, simply connected Riemannian manifold of dimension $d \geq 2$ and constant sectional curvature. Up to an isomorphism, space forms are equivalent to spherical (\mathbb{S}^d), Euclidean (\mathbb{E}^d), or hyperbolic spaces (\mathbb{H}^d) [35]. Distance geometry problems (DGPs) are concerned with finding an embedding for a set of pairwise measurements in a space form. DGP problems can be categorized as metric [25], nonmetric [16], or unlabeled [36–38], depending on the data modality and application domain. A nonmetric DGP aims to find x_1, \dots, x_N in a space form S , given a set of ordinal distance measurements $\mathcal{O} \subseteq [N]^4$ such that

$$\forall (n_1, n_2, n_3, n_4) \in \mathcal{O} : d(x_{n_1}, x_{n_2}) \leq d(x_{n_3}, x_{n_4}). \quad (1)$$

Although there exist theoretical results on the uniqueness of Euclidean embeddings [39] (up to an ordinal invariant transformation, i.e., an isotony), most often the underlying geometry of ordinal measurements is not known a priori [18, 40, 41].

We consider the problem of identifying the underlying space form from a given set of pairwise distance comparisons. For sufficiently many comparisons, this problem is equivalent to inferring geometrical information through the *sorted distance list* associated with ordinal measurements (1). A deterministic or a randomized binary sort algorithm needs at least $\Theta(\binom{N}{2} \log \binom{N}{2})$ pairwise comparisons to uniquely find the sorted distance list, if such a list exists [42]. Hence, we can define the *sorted index list* $(i_r, j_r)_{r \in \binom{N}{2}}$ according to

$$d(x_{i_1}, x_{j_1}) \geq \dots \geq d(x_{i_{\binom{N}{2}}}, x_{j_{\binom{N}{2}}}), \quad (2)$$

where $i_r < j_r$ for all $r \in \binom{N}{2}$ and all pairs of indices are distinct. Any geometry-related inference problem must be *invariant* with respect to arbitrary permutations of the point indices. In particular,

the pattern of the newly added indices in the sorted index list 2 is invariant to the permutations of point indices and has important geometrical implications. We formalize this notion in Definition 1.

Definition 1. The n -th ordinal spread of N points with a sorted index list is defined as

$$\forall n \in [N] : \alpha_n = \min \left\{ m \in \mathbb{N} : \text{card} \bigcup_{r=1}^m \{i_r, j_r\} \geq n \right\}.$$

Alternatively, the ordinal spread α_n is the rank of the first appearance of the n -th point in the sorted index list, i.e., $\text{card} \bigcup_{r=1}^{\alpha_n-1} \{i_r, j_r\} < n$, $\text{card} \bigcup_{r=1}^{\alpha_n} \{i_r, j_r\} \geq n$. As an example, for $d(x_1, x_2) \geq d(x_1, x_3) \geq \dots$, we have $\alpha_3 = 2$. From Definition 1, we observe that one can compute the ordinal spread α_n without knowing the point set positions, the distance and $\phi(\cdot)$ function or even the type of underlying space. Nevertheless, in Section 2.1 and later on, we use $\alpha_n(\{x_n\}_{n=1}^N)$ to denote the n -th ordinal spread computed for the points $\{x_n\}_{n=1}^N$ in a metric space.

In general, the ordinal spreads $\{\alpha_n\}_{n \in [N]}$ depend on the configuration of the underlying point set, up to a similarity preserving map [39]. In Proposition 1, we make the first step in studying ordinal spread variables by computing their range of possible values.

Proposition 1. For a set of $N \geq 4$ points with a given sorted index list, we have

- $\alpha_1 = \alpha_2 = 1, \alpha_3 = 2;$
- $4 \leq n \leq N : \lceil \frac{n}{2} \rceil \leq \alpha_n \leq \binom{n-1}{2} + 1.$

Clearly, the N -th ordinal spread variable, α_N , is the largest ordinal spread value which makes it a good choice for inferring geometry-related properties. In comparison, α_1, α_2 , and α_3 are fixed and independent on the space and hence noninformative (see the Supplement for more details). We next provide two illustrative examples that show how the ordinal spread α_N may be used to reveal the hyperbolic, Euclidean, and spherical geometry of the measurements. These results motivate the study of ordinal capacity.

2.1 Hyperbolicity of Trees

Hyperbolic spaces are space forms that offer small distortion when embedding trees [43, 44]. Here, we describe how to verify this hyperbolicity by using *ordinal spread random variables*. We generate a random tree T with the vertex set $V = [10^4]$. The maximum node degree is 3 and edge weights are i.i.d. realizations of a $\text{unif}(0, 1)$ -distributed random variable. Let $d_{m,n}$ be the distance between nodes m and n in V , defined as the sum of the weights on the unique path connecting the vertices. Then, we randomly subsample 10^6 different node subsets, or sub-cliques, of size $N \in \{10, 20\}$ ($N \ll |V| = 10^4$) as shown in Figure 1 (a). For each randomly selected sub-clique, we compute its N -th ordinal spread, α_N . Due to the inherently random nature of the clique selection process, α_N is a random variable which we term the ordinal spread random variable for the tree T . We can then compute the empirical distribution of the random variable, as illustrated in Figure 1(b_1, c_1). This motivates the following definition:

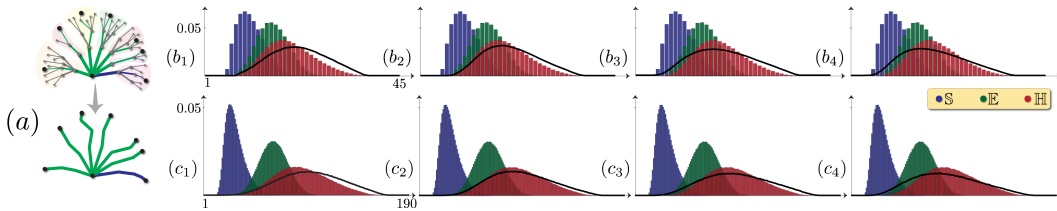


Figure 1: (a) Random selection of a sub-tree of size N . PMFs of α_{10} (top row) and α_{20} (bottom row) for random points in \mathbb{H}^2 (red), \mathbb{E}^2 (green), and \mathbb{S}^2 (blue). The black plots are empirical PMFs of α_N derived from (b_1, c_1) the noise-less tree T , (b_2, c_2) the additive noise contaminated tree, (b_3, c_3) the tree with permutation noise, and (b_4, c_4) a tree with both previous forms of noise.

Definition 2. Let S be a metric space, and P be a probability distribution on S . With a slight abuse of notation, we define the ordinal spread random variable α_N as

$$\forall N \in \mathbb{N} : \alpha_N = \alpha_N(X), X \sim P^{\otimes N}.$$

An ordinal spread random variable is defined with respect to the distribution P . Let us assume an *oracle* picks a set of distributions for embedded points in each space form, e.g., (projected) normal for hyperbolic and Euclidean spaces, and uniform distribution in the spherical space. The distribution of the corresponding ordinal spread random variable α_N is invariant with respect to scaling. More precisely, it is invariant to strongly isotonic point transformations (more information in the Supplement). As the results in Figure 1(b_1, c_1) indicate, the empirical distribution of α_N derived from a weighted tree T best matches (in the sense of total variation distance between the probability measures) with that of a random hyperbolic point set. For further verification, we repeated the same experiment for a random tree T with (1) additive measurements noise, e.g., $\tilde{d}_{m,n} = d_{m,n} + \eta$ where η is a sample of a zero-mean Gaussian noise (with 20 decibel signal-to-noise ratio), (2) random permutation noise for the sorted index lists, e.g., $\tilde{i} = \pi(i)$ and $\tilde{j} = \pi(j)$ where π is a permutation with average displacement of $|V| = 10^4$, and (3) both additive and permutation noise; see Figure 1(b_2, c_2), (b_3, c_3), and (b_4, c_4). The results clearly show that the distribution of the ordinal spread variable α_N is robust to noise and that it closely matches with that of a random hyperbolic point cloud. An important implication of this example is that ordinal spread variables can be used to determine the curvature sign of the underlying space. A more rigorous justification is provided in the subsequent exposition in Sections 3 and 4, where we formally connect the support of ordinal spread variables to a specific property of their underlying space forms, i.e., their *ordinal capacity*. In the Supplement, we show how to use ordinal capacity to compute a deterministic lower bound for the Euclidean embedding dimension of this tree.

2.2 Euclidean and Spherical Geometries of Cartographic Data

We describe next an experiment pertaining to the ordinal spread (random) variables of a similarity graph for geospatial data. The main idea is to use the distribution of these variables to show that the intrinsic geometry of small regions on the globe, which are “flat,” is close to Euclidean, whereas that of large regions, which are spread across the globe, are close to spherical.

We use three datasets: (1) 1,627 counties in the state of Illinois, (2) 11,954 counties in Midwestern states, and (3) 10^4 (subsampled) cities and towns across the world; refer to the Supplement for details on data sources. We construct the dissimilarity graph by computing the pairwise distances between the points using the Haversine formula, which determines the great-circle distance between two points on the globe given their longitudes and latitudes [45]. For each data set, we compute the empirical PMF of α_{20} from 10^6 randomly selected cliques of size 20 each; the results are shown in Figure 2. Comparing the PMFs for α_{20} and for random hyperbolic, Euclidean, and spherical points, we clearly observe the shift from an (approximately) Euclidean to a spherical geometry as the area spanned by the sampled points increases. We emphasize that these results are derived from distance comparisons only, since we discard the metric information in the distances.

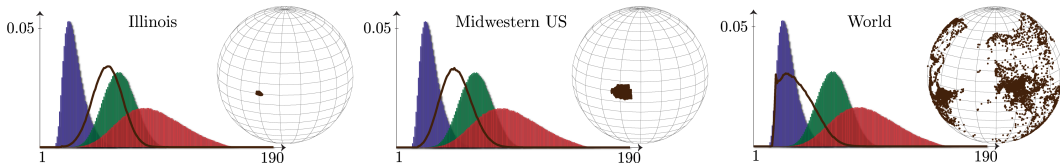


Figure 2: The empirical PMFs of α_{20} derived from subsampling the dissimilarity (distance) graph associated with points in the state of Illinois, across the Midwestern USA, and the world. Colored plots are PMFs of for random points in \mathbb{H}^2 (red), \mathbb{E}^2 (green), and \mathbb{S}^2 (blue).

3 The Ordinal Capacity

In the numerical experiment of Section 2.1, we discovered a distinguishing statistical behavior for the ordinal spread of randomly generated points in each possible space form. We show in what follows that this distinguishing pattern is related to the *capacity* of each space form to accommodate ordinal spread random variables with their underlying distributions. We define *ordinally dense sets* and show how they can help determine the support (the range of possible values) of the ordinal spread random variables in a space form¹.

Definition 3. Let $\{x_1, \dots, x_N\}$ be a set of distinct points in a metric space S . If

$$\exists n_0 \in [N] : \sup_{n \in [N] \setminus \{n_0\}} d(x_n, x_{n_0}) \leq \inf_{\{m, n\} \neq \subseteq [N] \setminus \{n_0\}} d(x_m, x_n),$$

then we say that $\{x_n\}_{n=1}^N$ is an *ordinally dense set* in S , or in short $\{x_n\}_{n=1}^N \subseteq S$.

In a nutshell, Definition 3 identifies point configurations that have a maximum possible ordinal spread. Intuitively, a set of N points is ordinally dense in S if and only if it has a subset of $N - 1$ points whose pairwise distances are **all** larger than (or equal to) their distances to the N -th point, i.e.,

$$\{x_n\}_{n=1}^N \subseteq S \iff \alpha_N \left(\{x_n\}_{n=1}^N \right) = \binom{N-1}{2} + 1. \quad (3)$$

The existence of an ordinally dense set of size N depends on the geometry of the underlying metric space, and is closely tied to what we term the *ordinal capacity* of the space (see Figure 3).

Definition 4. The *ordinal capacity* of a metric space S is defined as

$$K(S) = \sup \{ \text{card } \{x_n\} : \{x_n\} \subseteq S \}.$$

The ordinal capacity is an indicator of the capability of a metric space to realize an extremal pattern of point indices in the sorted index list (3). In the next theorem, we show that the ordinal capacity of a space form is intimately related to a spherical cap packing problem [47], which is concerned with the maximum number of non-overlapping spherical caps (or domes with a certain polar angle) in a hypersphere.

Theorem 1. Let N_d be the spherical $\frac{\pi}{6}$ -cap packing number of \mathbb{S}^d . The ordinal capacity of a space form S is given by

$$K(S) = \begin{cases} +\infty, & \text{if } S \cong \mathbb{H}^d \\ N_d + 1, & \text{if } S \cong \mathbb{E}^d, S \cong \mathbb{S}^d. \end{cases}$$

Theorem 1 shows that the ordinal capacity of space forms depends on their curvature sign and dimension. The ordinal capacity of a hyperbolic space is infinite, regardless of its dimension. This implies that for any $N \in \mathbb{N}$, there exists an ordinally dense hyperbolic point set $\{x_n\}_{n=1}^N$. In the Poincaré model, a centered regular $(N - 1)$ -gon with an additional point in the “center” is an ordinally

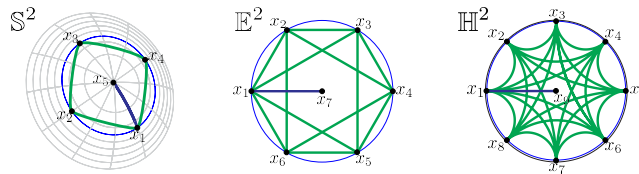


Figure 3: Ordinally dense point sets in 2-d space forms. As all distances in the (Euclidean) hexagon are greater than or equal to their distances to the center, the point set achieves the capacity $K(\mathbb{E}^2) = 7$.

¹We adopt Mirsky’s notation $\{m, n\} \neq$ for a set with two distinct elements m and n [46].

dense set (see Figure 3). In contrast, Euclidean and spherical spaces have *equal and finite* ordinal capacities. This finding is intuitively clear because any tangent space of \mathbb{S}^d is a linear space of dimension d , and the spherical distance converges to the ℓ_2 distance as the distance between the points diminishes. In the Supplement, we propose a refinement for the ordinal capacity of spherical spaces by imposing a minimum distance constraint for the point sets. We note that the current notion of ordinal capacity does not distinguish between hyperbolic spaces of different dimensions. Therefore, one may need to develop a more refined notion of ordinal capacity for hyperbolic spaces, e.g., based on extremal appearance patterns of *multiple* indices in the distance lists.

Using the previous result, we can numerically compute an upper bound on N_d, ρ_d , as a function of d , e.g. $\rho_1 = 2, \rho_2 = 6, \rho_3 = 15, \rho_4 = 31, \rho_5 = 59, \rho_6 = 106$ [47]. Note that the packing number N_d grows exponentially with the dimension d [48]. Hence, we have the following asymptotic bound for the ordinal capacity of a d -dimensional Euclidean (or spherical) space:

$$-\log\left(\frac{\sqrt{3}}{2}\right) + o(d) \leq \frac{1}{d} \log K(\mathbb{E}^d) \leq -\log\left(\frac{\sqrt{2}}{2}\right) + o(d).$$

4 The Support of Ordinal Spread Random Variables

In Section 2, we showed numerical evidence that ordinal spread random variables in Euclidean, spherical, and hyperbolic geometries have different supports. We therefore ask: *What is the maximum achievable ordinal spread, α_N , for a point set of size $N > K(S)$?* The answer to this question determines the support of ordinal spread random variables in Euclidean and spherical spaces, regardless of their underlying distribution P (see Definition 2). Note that since the ordinal capacity of a hyperbolic space is infinite, there always exists a point set of size N with maximum ordinal spread of $\binom{N-1}{2} + 1$ (see Proposition 1). For our subsequent analysis, we define the N -point ordinal spread of a space form S to be the maximum attainable ordinal spread α_N for the points in S . In Theorem 2, we express this quantity in terms of the ordinal capacity of S .

Theorem 2. *The N -point ordinal spread of a space form S is given by*

$$A_N(S) \stackrel{\text{def}}{=} \sup_{X \in S^N} \alpha_N(X) = E(T(N-1, K(S)-1)) + 1,$$

where $E(T(N, K))$ is the number of edges of $T(N, K)$, the K -partite Turán graph [49] with N vertices.

As a conclusion, the N -point ordinal spread of a space form, i.e., the support of its ordinal spread random variable α_N , depends on its ordinal capacity and the number of points N . For a space S with finite ordinal capacity, there exists a point set $X \in S^N$ such that $\alpha_N(X) < \binom{N-1}{2} + 1$. This holds if $N > K(S)$. With this result, we can revise the ordinal spread bound in Proposition 1.

Proposition 2. *For a set of $N \geq 4$ points in a space form S , we have*

$$\bullet \alpha_1 = \alpha_2 = 1, \alpha_3 = 2, \quad \bullet 4 \leq n \leq N : \left\lceil \frac{n}{2} \right\rceil \leq \alpha_n \leq A_n(S).$$

Theorem 2 and Proposition 2 explain in part the discriminatory ability of the support of ordinal spread random variables across different space forms. The N -point ordinal spread of a hyperbolic space \mathbb{H}^d is the maximum value possible, i.e., $A_N(\mathbb{H}^d) = \binom{N-1}{2} + 1$, regardless of its dimension. Even though the N -point ordinal spread of Euclidean and spherical spaces, \mathbb{E}^d and \mathbb{S}^d , varies with their dimension, they are equal to each other. This is evident from our distribution-free analysis of the ordinal capacity of these spaces (see Theorem 1 and its subsequent discussion). However, we can extend our distribution-free results to the following coarse lower bound for Euclidean (or spherical) embedding dimension of a similarity graph,

$$\min \left\{ d : \sup_{X \subseteq V : |X|=N} \alpha_N(X) \leq A_N(\mathbb{E}^d), \forall N \in [|V|] \right\} \leq d$$

where V is the vertex set of the graph. We may relax an exhaustive search over all 2^N vertex subsets, to a search over a random subselection of vertices. In the Supplement we use such a relaxation to compute a lower bound for the embedding dimension of the tree discussed in Section 2.1.

4.1 Visualizing Point Sets with Maximum Ordinal Spread

Here, we aim to gain geometrical intuition about the point sets with maximum ordinal spread in different space forms. To this end, we generate independent and identically distributed point sets from a (projected) normal distribution in 2-dimensional hyperbolic and Euclidean spaces. For each realization $\{x_n\}_{n=1}^N$, we compute the corresponding ordinal spread α_N . The maximum ordinal spread of the generated point sets, \hat{A}_N , gives an estimate for $A_N(\mathbb{E}^2)$ and $A_N(\mathbb{H}^2)$ (see Theorem 2). We repeat this experiment for varying size of the point sets $N \in \{4, 5, \dots, 13\}$.

For 5×10^5 realizations, we pick the point configurations with maximum ordinal spread; see Figure 4 (a, b). Recall that the point set with the theoretical maximum ordinal spread must have $N - 1$ points sampled from a sphere centered at the N -th point. So, we repeat this experiment by fixing a point at 0, and projecting the remaining points to their circumscribed circle, i.e., $\forall n \in [N - 1] : y_n = \frac{r}{\|x_n\|} x_n$, and $y_N = 0$, where $r = \max_{n \in [N-1]} \|x_n\|$. The randomly selected points $\{y_n\}_{n=1}^N$ produce a more accurate estimate for $A_N(\mathbb{H}^2)$ and $A_N(\mathbb{E}^2)$; see Figure 4 (c, d). For example, we have $\hat{A}_{13}(\mathbb{E}^2) = 56$, compared to the theoretical bound $A_{13}(\mathbb{E}^2) \leq 58$. Also, the estimated N -point ordinal spread of a hyperbolic space perfectly matches with the theoretical bound $A_N(\mathbb{H}^2) = \binom{N-1}{2} + 1$. The latter result is due to the capacity of hyperbolic spaces to host infinitely many ordinally dense point sets. Hence, the probability of randomly selecting an ordinally dense hyperbolic point set, of size N , is greater than its Euclidean counterpart.

Perhaps the most important observation is that the individual points in the extremal sets aggregate on nonoverlapping spherical caps of a circle, as seen in Figure 4 (c). The ordinal capacity of a space form equals the total number of such caps plus one (for the center point), i.e., $N_d + 1$. For example, there are 5 strictly non-overlapping spherical caps for 2-dimensional Euclidean space, whereas this number is infinite for hyperbolic spaces. Finally, these results illustrate that the N -th ordinal spread of each space form, $A_N(S)$, is the total number of edges in Turán graphs (see Theorems 1 and 2).

5 Numerical Experiments: Single-cell RNA Sequencing Data

Here, we focus on results pertaining to an important new data format omnipresent in computational molecular biology: *single-cell RNA sequencing* (scRNAseq) data. By using recently developed single-cell isolation and barcoding techniques, and by trading individual cell coverage for the number of cells captured, scRNA-seq data for the first time enables studying the activity patterns of millions of individual cells. This is in stark contrast with traditional bulk sequencing techniques that only provide *averaged snapshots* of cellular activity; scRNAseq measurements are also of special importance in cancer biology, as cancer cells are known to contain highly heterogeneous cell populations and the degree of heterogeneity carries significant information about disease progressions and the effectiveness of treatments [50]. Important for our study is the fact that due to the large number of different cells sequenced, cell measurements are extremely sparse and *imputed* in practice [51–53].

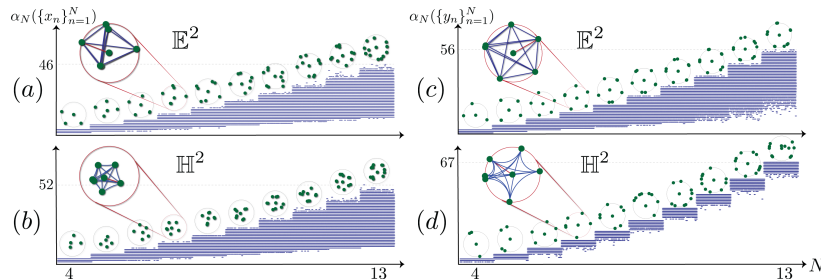


Figure 4: Ordinal spread of 5×10^5 i.i.d. point sets in \mathbb{E}^2 and \mathbb{H}^2 . For fixed N , we mark the set with the maximum ordinal spread: $\{x_n\}_{n=1}^N$ in Figures (a, b) and $\{y_n\}_{n=1}^N$ in Figures (c, d).

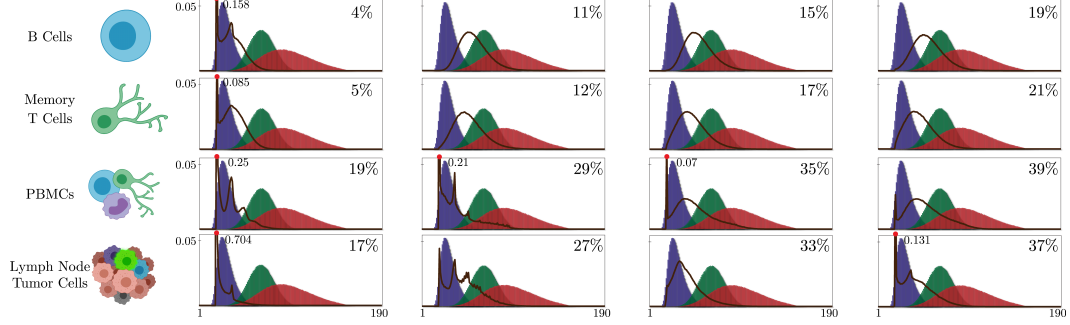


Figure 5: The empirical PMFs of α_{20} derived from subsampling the RFA similarity graph associated with scRNAseq data from homogeneous B cells ($\approx 10,000$ cells) and memory T cells ($\approx 10,000$), and heterogeneous PBMCs ($\approx 10,000$) and lymph node tumor cells ($\approx 3,000$). The left column shows the results for the raw data. From left to right, we increase the percentage of imputed data (densities are shown in the top-right corner).

Further, it has been pointed out [53, 54] that scRNA-seq data is very noisy due to biological stochasticity as well as dropouts and systemic noise. Existing methods for denoising and imputation of raw scRNA-seq data often involve building connection graphs among cells [52, 51] using the distance between cells to diffuse the expression profiles among neighboring cells and smooth out possible outliers. Thus, *relative expression differences (comparisons)*, rather than *absolute expression values*, enable more accurate biological data mining via clustering, lineage detection, or inference of pseudotemporal orderings of cells [55]. As an example, [18] constructs similarity probabilities from a relative forest accessibility (RFA) matrix [56] and uses the obtained values to suggest that hyperbolic spaces are more suitable than Euclidean spaces for scRNAseq data embedding. We illustrate next that identifying the geometric properties of scRNAseq data using comparisons also provides unique information about the diversity of cellular populations [50], outliers and the properties of imputation methods. Furthermore, since scRNA captures temporal hierarchical information about cells, as well as the cyclic nature of cell cycles, we expect spherical space forms to be equally useful as hyperbolic space forms in the process of embedding. To this end, we compute the empirical distribution of ordinal spread random variables associated with scRNA lymphoma (cancer) cells and cell *families* known as mononuclear cells (PBMCs), comprising T cells, B cells, and monocytes, which are often targeted in cancer immunotherapy. In this case, as illustrated by our numerical findings in Figure 5, these distributions contain peaks for small values that indicate that the data is sparse and contains outliers or highly heterogeneous cellular populations. Intuitively, probability peaks for small values of α_N arise when newly added indices in the ordered distance list appear in quick succession which can be attributed to one or multiple points at large distance from the remaining points (outliers); for more details see the Supplement. As imputation adds new data points by using averaged and smoothed information of observed measurements, it is expected to remove peaks in the aforementioned distributions, which is clearly the case for homogeneous cellular populations, but not for cancer cells and PBMCs. The reason why imputation does not remove peaks for the latter two categories can be attributed to the fact that the peaks arise due to the presence of many different cell types (e.g., recall that PBMCs contain B, T and monocytes and consequently, multiple peaks are observed in the ordinal spread distributions of raw data) which cannot and should not be smoothed out to form one class as this defeats the purpose of using single-cell measurements. Equally importantly, the results show that the Magic imputation software we used [51] imputes information into the noisy measurements without changing the geometry of the data, which is an important indicator of the quality of the procedure. Our next results pertain to the actual embedding quality of the measured similarities. We consider nonmetric embeddings [25, 16] of RFA scores of scRNAseq data from adult

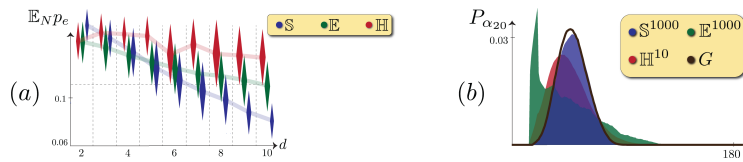


Figure 6: (a) PMFs of α_{20} from the RFA similarity graph (G) vs. random points in space forms of optimal dimensions. (b) $\mathbb{E}_N p_e$ for embedded points in d -dimensional space forms.

planarians [55]. The data set contains $N \approx 26,000$ cells with gene expression vectors of dimension $d \approx 21,000$. In Figure 6 (a), we report the empirical probability of incorrect comparison $\mathbb{E}_N p_e$ for embedding RFA similarities in different space forms of varying dimensions. The results thus confirm that a *spherical* geometry is actually better suited for accurate nonmetric embeddings, which supports the frequently ignored understanding that cells are measured at various stages of the same cell cycle. For our analysis, we compute $\hat{P}_{\alpha_{20}}$ from the similarity graph G . Due to the heavy-tailed nature of the original data distribution, we choose (oracle) log-normal distributions for the points in each space form. Then, we repeat the experiments for various dimensions and each space form/distribution parameters to find the closest ordinal spread variable to $\hat{P}_{\alpha_{20}}$. From Figure 6 (b), we conclude that an ordinal spread variable from a high-dimensional ($\approx 1,000$) *spherical space* best matches $\hat{P}_{\alpha_{20}}$. For the details about the embedding methods, datasets, and further discussions refer to the Supplement.

References

- [1] Josep M Porta, Lluís Ros, Federico Thomas, and Carme Torras. A branch-and-prune solver for distance constraints. *IEEE Transactions on Robotics*, 21(2):176–187, 2005.
- [2] Puoya Tabaghi, Ivan Dokmanić, and Martin Vetterli. Kinetic Euclidean distance matrices. *IEEE Transactions on Signal Processing*, 68:452–465, 2019.
- [3] Anthony Man-Cho So and Yinyu Ye. Theory of semidefinite programming for sensor network localization. *Mathematical Programming*, 109(2-3):367–384, 2007.
- [4] Gordon M Crippen, Timothy F Havel, et al. *Distance geometry and molecular conformation*, volume 74. Research Studies Press Taunton, 1988.
- [5] Leo Liberti, Carlile Lavor, Nelson Maculan, and Antonio Mucherino. Euclidean distance geometry and applications. *SIAM review*, 56(1):3–69, 2014.
- [6] Ivan Dokmanic, Reza Parhizkar, Juri Ranieri, and Martin Vetterli. Euclidean distance matrices: Essential theory, algorithms, and applications. *IEEE Signal Processing Magazine*, 32(6):12–30, 2015.
- [7] Kevin Verbeek and Subhash Suri. Metric embedding, hyperbolic space, and social networks. In *Proceedings of the thirtieth annual symposium on Computational geometry*, pages 501–510, 2014.
- [8] Pan Li and Olgica Milenkovic. Inhomogeneous hypergraph clustering with applications. *arXiv preprint arXiv:1709.01249*, 2017.
- [9] Michael Ashburner, Catherine A Ball, Judith A Blake, David Botstein, Heather Butler, J Michael Cherry, Allan P Davis, Kara Dolinski, Selina S Dwight, Janan T Eppig, et al. Gene ontology: tool for the unification of biology. *Nature genetics*, 25(1):25–29, 2000.
- [10] Matt Le, Stephen Roller, Laetitia Papaxanthos, Douwe Kiela, and Maximilian Nickel. Inferring concept hierarchies from text corpora via hyperbolic embeddings. *arXiv preprint arXiv:1902.00913*, 2019.
- [11] Richard C Wilson, Edwin R Hancock, Elżbieta Pękalska, and Robert PW Duin. Spherical embeddings for non-Euclidean dissimilarities. In *2010 IEEE Computer Society Conference on Computer Vision and Pattern Recognition*, pages 1903–1910. IEEE, 2010.
- [12] Robin M Green and Robin Michael Green. *Spherical astronomy*. Cambridge University Press, 1985.
- [13] Shuanghua Bai, Huo-Duo Qi, and Naihua Xiu. Constrained best Euclidean distance embedding on a sphere: a matrix optimization approach. *SIAM Journal on Optimization*, 25(1):439–467, 2015.
- [14] Asi Elad, Yosi Keller, and Ron Kimmel. Texture mapping via spherical Multi-dimensional Scaling. In *International Conference on Scale-Space Theories in Computer Vision*, pages 443–455. Springer, 2005.

- [15] Joseph B Kruskal. Nonmetric Multidimensional Scaling: a numerical method. *Psychometrika*, 29(2):115–129, 1964.
- [16] Sameer Agarwal, Josh Wills, Lawrence Cayton, Gert Lanckriet, David Kriegman, and Serge Belongie. Generalized non-metric multidimensional scaling. In *Artificial Intelligence and Statistics*, pages 11–18, 2007.
- [17] Chad Giusti, Eva Pastalkova, Carina Curto, and Vladimir Itskov. Clique topology reveals intrinsic geometric structure in neural correlations. *Proceedings of the National Academy of Sciences*, 112(44):13455–13460, 2015.
- [18] Anna Klimovskaia, David Lopez-Paz, Léon Bottou, and Maximilian Nickel. Poincaré maps for analyzing complex hierarchies in single-cell data. *Nature Communications*, 11(1):1–9, 2020.
- [19] Çağatay Demiralp, Michael S Bernstein, and Jeffrey Heer. Learning perceptual kernels for visualization design. *IEEE transactions on visualization and computer graphics*, 20(12):1933–1942, 2014.
- [20] Daniel J Navarro and Michael D Lee. Common and distinctive features in stimulus similarity: A modified version of the contrast model. *Psychonomic Bulletin & Review*, 11(6):961–974, 2004.
- [21] Roger N Shepard. The analysis of proximities: Multidimensional Scaling with an unknown distance function. i. *Psychometrika*, 27(2):125–140, 1962.
- [22] Roger N Shepard. The analysis of proximities: Multidimensional Scaling with an unknown distance function. ii. *Psychometrika*, 27(3):219–246, 1962.
- [23] Laurens Van Der Maaten and Kilian Weinberger. Stochastic triplet embedding. In *2012 IEEE International Workshop on Machine Learning for Signal Processing*, pages 1–6. IEEE, 2012.
- [24] Omer Tamuz, Ce Liu, Serge Belongie, Ohad Shamir, and Adam Tauman Kalai. Adaptively learning the crowd kernel. *arXiv preprint arXiv:1105.1033*, 2011.
- [25] Puoya Tabaghi and Ivan Dokmanić. Hyperbolic distance matrices. In *Proceedings of the 26th ACM SIGKDD International Conference on Knowledge Discovery & Data Mining*, page 1728–1738, 2020.
- [26] Amos Tanay and Aviv Regev. Scaling single-cell genomics from phenomenology to mechanism. *Nature*, 541(7637):331–338, 2017.
- [27] Fabian Wauthier, Michael Jordan, and Nebojsa Jojic. Efficient ranking from pairwise comparisons. In *International Conference on Machine Learning*, pages 109–117, 2013.
- [28] Kevin G Jamieson and Robert Nowak. Active ranking using pairwise comparisons. In *Advances in Neural Information Processing Systems*, pages 2240–2248, 2011.
- [29] Kevin G Jamieson and Robert D Nowak. Low-dimensional embedding using adaptively selected ordinal data. In *2011 49th Annual Allerton Conference on Communication, Control, and Computing (Allerton)*, pages 1077–1084. IEEE, 2011.
- [30] Siavash Haghir, Debarghya Ghoshdastidar, and Ulrike von Luxburg. Comparison-based nearest neighbor search. In *Artificial Intelligence and Statistics*, pages 851–859, 2017.
- [31] Siavash Haghir, Damien Garreau, and Ulrike Luxburg. Comparison-based random forests. In *International Conference on Machine Learning*, pages 1871–1880, 2018.
- [32] Zhenghang Cui, Nontawat Charoenphakdee, Issei Sato, and Masashi Sugiyama. Classification from triplet comparison data. *Neural Computation*, 32(3):659–681, 2020.
- [33] Gunnar Carlsson. Topology and data. *Bulletin of the American Mathematical Society*, 46(2):255–308, 2009.
- [34] Yuansheng Zhou, Brian H Smith, and Tatyana O Sharpee. Hyperbolic geometry of the olfactory space. *Science advances*, 4(8):eaq1458, 2018.

- [35] John M Lee. *Riemannian Manifolds: An Introduction to Curvature*. Springer New York, 2007.
- [36] Steven S Skiena, Warren D Smith, and Paul Lemke. Reconstructing sets from interpoint distances. In *Proceedings of the sixth annual symposium on Computational geometry*, pages 332–339, 1990.
- [37] Neil C Jones, Pavel A Pevzner, and Pavel Pevzner. *An introduction to bioinformatics algorithms*. MIT press, 2004.
- [38] Shuai Huang and Ivan Dokmanić. Reconstructing point sets from distance distributions. *arXiv preprint arXiv:1804.02465*, 2018.
- [39] Matthäus Kleindessner and Ulrike Luxburg. Uniqueness of ordinal embedding. In *Conference on Learning Theory*, pages 40–67, 2014.
- [40] Qiong Cao, Yiming Ying, and Peng Li. Similarity metric learning for face recognition. In *Proceedings of the IEEE international conference on computer vision*, pages 2408–2415, 2013.
- [41] Brian McFee, Gert Lanckriet, and Tony Jebara. Learning multi-modal similarity. *Journal of machine learning research*, 12(2), 2011.
- [42] Thomas H Cormen, Charles E Leiserson, Ronald L Rivest, and Clifford Stein. *Introduction to algorithms*. MIT press, 2009.
- [43] Rik Sarkar. Low distortion delaunay embedding of trees in hyperbolic plane. In *International Symposium on Graph Drawing*, pages 355–366. Springer, 2011.
- [44] Octavian Ganea, Gary Bécigneul, and Thomas Hofmann. Hyperbolic entailment cones for learning hierarchical embeddings. In *International Conference on Machine Learning*, pages 1646–1655. PMLR, 2018.
- [45] Glen Van Brummelen. *Heavenly mathematics: The forgotten art of spherical trigonometry*. Princeton University Press, 2012.
- [46] Leonid Mirsky. *Transversal Theory: An account of some aspects of combinatorial mathematics*. Academic Press, 1971.
- [47] Robert Alexander Rankin. The closest packing of spherical caps in n dimensions. *Glasgow Mathematical Journal*, 2(3):139–144, 1955.
- [48] Aaron D Wyner. Random packings and coverings of the unit n -sphere. *The Bell System Technical Journal*, 46(9):2111–2118, 1967.
- [49] Pál Turán. On an external problem in graph theory. *Mat. Fiz. Lapok*, 48:436–452, 1941.
- [50] Corbin E Meacham and Sean J Morrison. Tumour heterogeneity and cancer cell plasticity. *Nature*, 501(7467):328–337, 2013.
- [51] David van Dijk, Juozas Nainys, Roshan Sharma, Pooja Kaithail, Ambrose J Carr, Kevin R Moon, Linas Mazutis, Guy Wolf, Smita Krishnaswamy, and Dana Pe’er. Magic: A diffusion-based imputation method reveals gene-gene interactions in single-cell rna-sequencing data. *BioRxiv*, page 111591, 2017.
- [52] Wei Vivian Li and Jingyi Jessica Li. An accurate and robust imputation method scimpute for single-cell rna-seq data. *Nature communications*, 9(1):1–9, 2018.
- [53] Stephanie C Hicks, F William Townes, Mingxiang Teng, and Rafael A Irizarry. Missing data and technical variability in single-cell RNA-sequencing experiments. *Biostatistics*, 19(4):562–578, 2018.
- [54] Gökçen Eraslan, Lukas M Simon, Maria Mircea, Nikola S Mueller, and Fabian J Theis. Single-cell RNA-seq denoising using a deep count autoencoder. *Nature communications*, 10(1):1–14, 2019.

- [55] Mireya Plass, Jordi Solana, F Alexander Wolf, Salah Ayoub, Aristotelis Misios, Petar Glažar, Benedikt Obermayer, Fabian J Theis, Christine Kocks, and Nikolaus Rajewsky. Cell type atlas and lineage tree of a whole complex animal by single-cell transcriptomics. *Science*, 360(6391), 2018.
- [56] P CHEBOTAREV and EV SHAMIS. The matrix-forest theorem and measuring relations in small social groups. *Automation and remote control*, 58(9):1505–1514, 1997.
- [57] Grace XY Zheng, Jessica M Terry, Phillip Belgrader, Paul Ryvkin, Zachary W Bent, Ryan Wilson, Solongo B Ziraldo, Tobias D Wheeler, Geoff P McDermott, Junjie Zhu, et al. Massively parallel digital transcriptional profiling of single cells. *Nature communications*, 8(1):1–12, 2017.
- [58] Hodgkin’s Lymphoma, Dissociated Tumor: Targeted-Compare, Immunology Panel by Cell Ranger 4.0.0. *10x Genomics*, July 7th, 2020.
- [59] PBMCs from a Healthy Donor: Targeted, Immunology Panel by Cell Ranger 4.0.0. *10x Genomics*, July 7th, 2020.
- [60] Yukiteru Ono, Kiyoshi Asai, and Michiaki Hamada. PBSIM: PacBio reads simulator—toward accurate genome assembly. *Bioinformatics*, 29(1):119–121, 2013.

SUPPLEMENTARY MATERIALS

Contents

1	Introduction	1
1.1	Related Works	2
2	The Ordinal Spread	3
2.1	Hyperbolicity of Trees	4
2.2	Euclidean and Spherical Geometries of Cartographic Data	5
3	The Ordinal Capacity	6
4	The Support of Ordinal Spread Random Variables	7
4.1	Visualizing Point Sets with Maximum Ordinal Spread	8
5	Numerical Experiments: Single-cell RNA Sequencing Data	8
6	PROOFS OF THEOREMS AND PROPOSITIONS	15
6.1	Proof of Proposition 1	15
6.2	Proof of Theorem 1	16
6.2.1	Hyperbolic space	16
6.2.2	Euclidean space	17
6.2.3	Spherical space	18
6.3	Proof of Theorem 2	20
6.4	Proof of Proposition 2	21
7	NUMERICAL EXPERIMENTS	21
7.1	Datasets	21
7.2	Hyperbolicity of Trees	22
7.2.1	On Euclidean Embedding Dimension of Trees	25
7.3	Single-cell RNA Expression Data	26
8	EMBEDDING ALGORITHMS	28
8.1	Hyperbolic Embedding	28
8.2	Spherical Embedding	29
8.3	Euclidean Embedding	30

6 PROOFS OF THEOREMS AND PROPOSITIONS

Notation For any two numbers $a, b \in \mathbb{R}$, we let $a \vee b$ and $a \wedge b$ be their maximum and minimum. We use small letters for vectors, $x \in \mathbb{R}^m$, and capital letters for matrices, $X = (x_{i,j}) \in \mathbb{R}^{m \times n}$. We denote the m -th standard basis vector in \mathbb{R}^M by e_m , $m \in [M]$ and let $[M]$ be short for the set $\{1, \dots, M\}$. For vectors $x, y \in \mathbb{R}^{d+1}$, their dot product is denoted by $\langle x, y \rangle$, and their Lorentzian inner product is $[x, y] = -x_0 y_0 + \sum_{i=1}^d x_i y_i$. The d -dimensional 'Loid model of hyperbolic space is a Riemannian manifold $\mathbb{L}^d = \{x \in \mathbb{R}^d : [x, x] = -1\}$ with the distance function given by $d(x, y) = \text{acosh}(-[x, y])$. Finally, 0 and 1 are all-zero and all-one vectors of appropriate dimensions. Let C be a subset of a space form (S, d) , and $x \in S$; We define

$$d_{\min}(C) = \inf \{d(x, y) : x, y \in C, x \neq y\},$$

$$d_{\max}(x, C) = \sup \{d(x, y) : y \in C\}.$$

The cardinality of a discrete set C is denoted by $\text{card } C$. The graph-theoretic notations simplifies the main results of this paper. For a graph G , we denote its edge set as $E(G)$. Let G_{p_1, \dots, p_K} be a complete K -partite graph with part sizes p_1, \dots, p_K . The Turán graph [49] $T(N, K)$ is a complete K -partite graph with N vertices, and part sizes²

$$p_k = \begin{cases} N_1 + 1, & \text{for } 1 \leq k \leq K_1 \\ N_1, & \text{for } K_1 + 1 \leq k \leq K. \end{cases}$$

Then, $\text{card } E(T(N, K)) = \binom{N}{2} - K_1 \binom{N_1+1}{2} - (K - K_1) \binom{N_1}{2}$.³

6.1 Proof of Proposition 1

From Definition 1, the values for $\alpha_1(X)$, $\alpha_2(X)$ and $\alpha_3(X)$ are trivial. The lower bound for $\alpha_N(X)$ simply follows from the uniqueness of pairwise distances. To put formally, we have

$$\alpha_N(X) = \min \left\{ m \in \mathbb{N} : \text{card} \bigcup_{r=1}^m \{i_r, j_r\} = N \right\} \geq \left\lceil \frac{N}{2} \right\rceil.$$

For the upper bound, $\alpha_N(X)$ is maximum when all $N - 1$ smallest pairwise distances are incident to a unique point; see Figure 2 (b). The total length of the distance list is $\binom{N}{2}$. Therefore, we have

$$\alpha_N(X) \leq \binom{N}{2} - (N - 1) + 1 = \binom{N - 1}{2} + 1.$$

Remark. Let us devise an experiment to show how the k -th ordinal spread can distinguish space forms. We randomly generate i.i.d. points $\{x_n\}_{n=1}^N$ from absolutely continuous distributions with full support in hyperbolic, Euclidean and spherical spaces.⁴ In Figure 7, we plot the k -th ordinal spread α_k for each realization $\{x_n\}_{n=1}^N$. We find the empirical maximum of α_N to be the most sensitive indicator of the geometry of underlying space. While the emerging pattern of α_N 's is dependent on the distribution of point sets, the behavior of empirical maximum of N -th ordinal spread is robust to the choice of point set distributions, as it converges to its supremum almost surely. Therefore, we introduce the *N -point ordinal spread* for a metric space – a tool to categorize space forms based on their ability to house extremal ordinal patterns, in the sense of Theorem 2.

²From $\sum_{k=1}^K p_k = N$, we have $N_1 = \lfloor \frac{N}{K} \rfloor$, $K_1 = N - KN_1$.

³This is simplified from $\text{card } E(G_{p_1, \dots, p_K}) = \binom{N}{2} - \sum_{k=1}^K \binom{p_k}{2}$. For $K > N$, we assume the graph is complete and $E(T(N, K)) = \binom{N}{2}$.

⁴Uniform distribution for spherical, and projected normal for hyperbolic space, i.e., $y = [\sqrt{1 + \|x\|^2}, x^\top]^\top$ where $x \sim \mathcal{N}(0, \sigma^2 I)$.

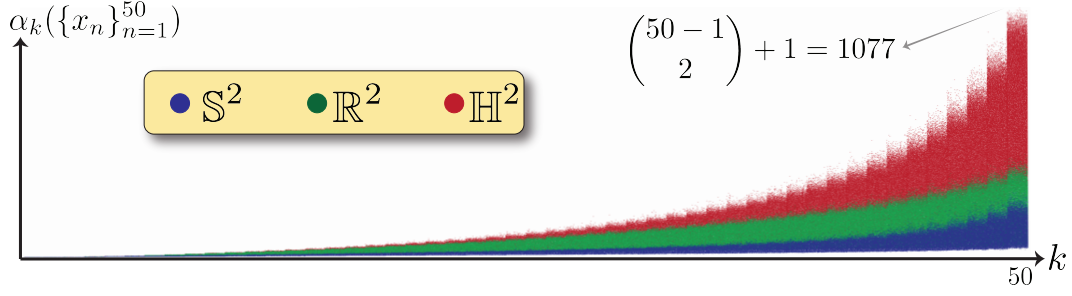


Figure 7: The k -th ordinal spread of 10^5 randomly generated points $\{x_n\}_{n=1}^{50}$ in 2-dimensional space forms.

6.2 Proof of Theorem 1

Let us separately consider hyperbolic, Euclidean, and spherical spaces.

6.2.1 Hyperbolic space

Let $r \in \mathbb{R}^+$, and $x_1(r), \dots, x_N(r) \in \mathbb{L}^d$ be a set of parameterized points in 'Loid model of d -dimensional hyperbolic space, such that

$$\forall n \in [N] : x_n(r) = \begin{bmatrix} \sqrt{1 + \|y_n(r)\|^2} \\ y_n(r) \end{bmatrix},$$

where $y_N(r) = 0$, and $y_i(r)^\top y_j(r) = r^2 \cos 2\pi \frac{|i-j|}{N-1}$, $\forall i, j \in [N-1]$. To see an example, see Figure 8. For these data points, we have

$$d_{\min}(\{x_n(r)\}_{n=1}^{N-1}) = \operatorname{acosh} \left(1 + r^2 (1 - \cos \frac{2\pi}{N-1}) \right),$$

$$d_{\max}(\{x_n(r)\}_{n=1}^{N-1}, x_N(r)) = \operatorname{acosh}(\sqrt{1 + r^2}).$$

Therefore, for any $N \in \mathbb{N}$, there exists a $r \in \mathbb{R}^+$ such that $\{x_n(r)\}_{n=1}^N \subseteq \mathbb{L}^d$. Hence,

$$\begin{aligned} K(\mathbb{L}^d) &= \sup \left\{ N : \{x_n(r)\}_{n=1}^N \subseteq \mathbb{L}^d \right\} \\ &= \infty. \end{aligned}$$

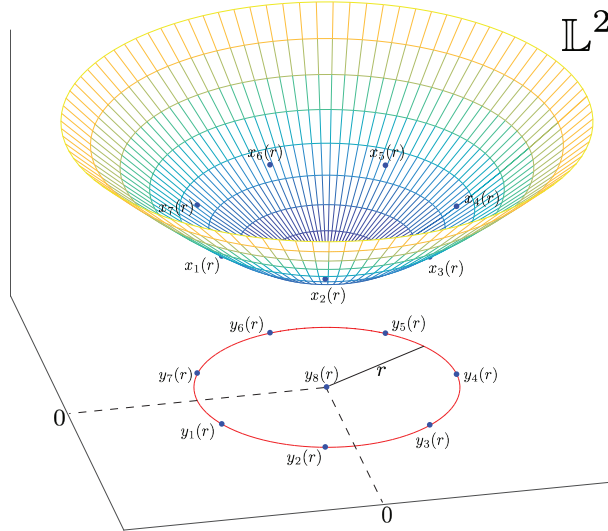


Figure 8: An example of $N = 8$ parameterized points $\{x_n(r)\}_{n=1}^N$ in \mathbb{L}^2 and $\{y_n(r)\}_{n=1}^N$ in \mathbb{R}^2 .

This result hold for all dimensions $d \geq 2$.

6.2.2 Euclidean space

Lemma 1. *There is a set of points x_1, \dots, x_N in \mathbb{R}^d such that*

$$\forall n \in [N-1] : \|x_n - x_N\| = 1,$$

where $d_{\max}(x_N, \{x_n\}_{n=1}^{N-1}) \leq d_{\min}(\{x_n\}_{n=1}^{N-1})$ and $N = K(\mathbb{R}^d)$.

Proof. Let $\{y_n\}_{n=1}^N$ be a set of points in \mathbb{R}^d such that

$$d_{\max}(y_N, \{y_n\}_{n=1}^{N-1}) \leq d_{\min}(\{y_n\}_{n=1}^{N-1}),$$

or $\alpha_N(\{y_n\}_{n=1}^N) = \binom{N-1}{2} + 1$. Without loss of generality, we assume $y_N = 0$ and $d_{\max}(y_N, \{y_n\}_{n=1}^{N-1}) = 1$. Let $x_n = \frac{1}{\|y_n\|} y_n$, $\forall n \in [N-1]$ and $x_N = y_N$. We want to show that $\alpha_N(\{x_n\}_{n=1}^N) \geq \alpha_N(\{y_n\}_{n=1}^N)$. Following the definition of ordinal spread, we have

$$\begin{aligned} \alpha_N(\{x_n\}_{n=1}^N) &\stackrel{(a)}{\geq} \text{card} \left\{ (i, j) : d(x_i, x_j) \geq d_{\max}(x_N, \{x_n\}_{n=1}^{N-1}), i, j \in [N-1], i > j \right\} + 1, \\ &\stackrel{(b)}{=} \text{card} \left\{ (i, j) : d(x_i, x_j) \geq 1, i, j \in [N-1], i > j \right\} + 1, \\ &\stackrel{(c)}{\geq} \text{card} \left\{ (i, j) : d(y_i, y_j) \geq 1, i, j \in [N-1], i > j \right\} + 1, \\ &= \alpha_N(\{y_n\}_{n=1}^N) \end{aligned}$$

where (a) holds with equality if x_N appears last in the sorted distance list, i.e., if $x_N = x_{(N)}$, (b) is due to $d_{\max}(x_N, \{x_n\}_{n=1}^{N-1}) = 1 = d_{\max}(y_N, \{y_n\}_{n=1}^{N-1})$. To prove inequality (c), let $d(y_i, y_j) \geq 1$ for distinct $i, j \in [N-1]$. Then,

$$\begin{aligned} d(y_i, y_j)^2 &= \frac{\|y_i\| - 1}{\|y_i\|} \left(\|y_i - y_j\|^2 - \|y_j\|^2 + \|y_i\|^2 \right) + \left\| \frac{1}{\|y_i\|} y_i - y_j \right\|^2 \\ &= \frac{d(y_N, y_i) - 1}{\|y_i\|} \left(d(y_i, y_j)^2 - d(y_N, y_j)^2 + d(y_N, y_i) \right) + \left\| \frac{1}{\|y_i\|} y_i - y_j \right\|^2 \\ &\stackrel{(a)}{\leq} \left\| \frac{1}{\|y_i\|} y_i - y_j \right\|^2 \\ &\stackrel{(b)}{\leq} \left\| \frac{1}{\|y_i\|} y_i - \frac{1}{\|y_j\|} y_j \right\|^2 \\ &= d(x_i, x_j)^2 \end{aligned}$$

where (a) follows from $d(y_N, y_i) \leq 1$, $d(y_N, y_j) \leq 1$, $d(y_i, y_j)^2 \geq 1$, and (b) follows from the symmetry in the argument. Therefore, we have

$$\{(i, j) : d(y_i, y_j) \geq 1, i, j \in [N-1], i > j\} \subseteq \{(i, j) : d(x_i, x_j) \geq 1, i, j \in [N-1], i > j\}.$$

Hence, $\{x_n\}_{n=1}^N$ is an ordinally dense subset of \mathbb{R}^d . \square

From Lemma 1, we want find an ordinally dense set of points x_1, \dots, x_N in \mathbb{R}^d such that

$$\forall n \in [N-1] : \|x_n\| = 1, \text{ and } x_N = 0.$$

From the definition of ordinal spread, we have

$$\begin{aligned} \alpha_N(\{x_n\}_{n=1}^N) &= \text{card} \left\{ (i, j) : d(x_i, x_j) \geq d_{\max}(x_N, \{x_n\}_{n=1}^{N-1}), i, j \in [N-1], i > j \right\} + 1, \\ &= \text{card} \left\{ (i, j) : \|x_i\|^2 + \|x_j\|^2 - 2x_i^\top x_j \geq 1^2, i, j \in [N-1], i > j \right\} + 1, \\ &= \text{card} \left\{ (i, j) : \text{acos}(x_i^\top x_j) \geq \frac{\pi}{3}, i, j \in [N-1], i > j \right\} + 1. \end{aligned}$$

We can find a maximum number of ordinally dense points by solving a spherical cap packing problem; see Figure 9.

Definition 5. Let \mathbb{S}^{d-1} be the $(d-1)$ -dimensional unit sphere in \mathbb{R}^d . We define the spherical α -cap $C_x(\alpha)$ as

$$C_x(\alpha) = \{y \in \mathbb{S}^{d-1} : x^\top y < \cos(\alpha)\},$$

for any $x \in \mathbb{S}^{d-1}$.

Definition 6. The maximum number of non-overlapping $C_x(\alpha)$ is defined as

$$N(\alpha) = \max_{N \in \mathbb{N}} \left\{ N : \exists x_1, \dots, x_N \in \mathbb{S}^{d-1} \text{ such that } \bigcup_{j \in \mathcal{I}, j \neq i} C_{x_j}(\alpha) \cap C_{x_i}(\alpha) = \emptyset, \forall \mathcal{I} \subseteq [N], \forall i \in [N] \right\}.$$

Therefore, we have

$$\begin{aligned} K(\mathbb{R}^d) &= \sup \{ \text{card} \{x_n\} : \{x_n\} \subseteq \mathbb{R}^d \}, \\ &= \sup \left\{ N : x_1, \dots, x_N \in \mathbb{R}^d, \alpha_N \left(\{x_n\}_{n=1}^N \right) = \binom{N-1}{2} + 1 \right\}, \\ &= \sup \left\{ N : x_1, \dots, x_N \in \mathbb{R}^d, \text{card} \left\{ (i, j) : \text{acos}(x_i^\top x_j) \geq \frac{\pi}{3}, i, j \in [N-1], i > j \right\} = \binom{N-1}{2} \right\}, \\ &= \sup \left\{ N : x_1, \dots, x_N \in \mathbb{R}^d \text{ such that } \text{acos}(x_i^\top x_j) \geq \frac{\pi}{3}, i, j \in [N], i \neq j \right\} + 1, \\ &\stackrel{(a)}{=} N\left(\frac{\pi}{6}\right) + 1, \\ &\stackrel{(b)}{\leq} \left\lfloor \sqrt{\frac{\pi}{8}} \frac{\Gamma\left(\frac{d-1}{2}\right)}{\Gamma\left(\frac{d}{2}\right) \int_0^{\frac{\pi}{4}} \sin^{d-2} \theta \left(\cos \theta - \frac{\sqrt{2}}{2}\right) d\theta} \right\rfloor + 1, \end{aligned}$$

where (a) follows from a simple illustration in Figure 9, and (b) is given in [47]. For large d , Rankin provided the following approximation,

$$N(\alpha) \sim \frac{(\frac{1}{2}\pi d^3 \cos 2\alpha)^{\frac{1}{2}}}{(\sqrt{2} \sin \alpha)^{d-1}}.$$

Therefore, we have $N(\frac{\pi}{6}) \sim \sqrt{\pi} d^{\frac{3}{2}} 2^{\frac{d-3}{2}} = C \exp \left\{ -d \log \frac{\sqrt{2}}{2} + \frac{3}{2} \log d \right\}$ for some constant C . The maximum number of non-overlapping spherical caps of half angle θ which can be placed on the unit sphere in \mathbb{R}^d is not less than $\exp(-d \log \sin 2\theta + o(d))$ [48]. Therefore, the lower bound on $N(\frac{\pi}{6})$ is given by $\exp(-d \log \frac{\sqrt{3}}{2} + o(d))$.

6.2.3 Spherical space

Lemma 2. There is a set of points x_1, \dots, x_N in \mathbb{S}^d such that

$$\forall n \in [N-1] : d(x_n, x_N) = \text{acos}(1 - \epsilon),$$

where $d_{\max}(x_N, \{x_n\}_{n=1}^{N-1}) \leq d_{\min}(\{x_n\}_{n=1}^{N-1})$, $N = K(\mathbb{S}^d)$, and for some $\epsilon \geq 0$.

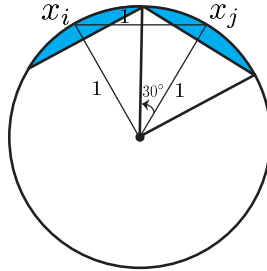


Figure 9: Spherical $\frac{\pi}{6}$ -cap packing on the surface of a unit sphere \mathbb{S}^1 .

Proof. Let $\{y_n\}_{n=1}^N$ be a set of points in \mathbb{S}^d such that

$$d_{\max}(y_N, \{y_n\}_{n=1}^{N-1}) \leq d_{\min}(\{y_n\}_{n=1}^{N-1}),$$

or $\alpha_N(\{y_n\}_{n=1}^N) = \binom{N-1}{2} + 1$. Without loss of generality, we assume $\alpha_N(\{y_n\}_{n=1}^N) = \binom{N-1}{2} + 1$, $y_N = e_1$,⁵ and $d_{\max}(y_N, \{y_n\}_{n=1}^{N-1}) = \text{acos}(1 - \epsilon)$. From the latter condition, we have

$$y_n \stackrel{\text{def}}{=} \begin{bmatrix} \sqrt{1 - \|z_n\|^2} \\ z_n \end{bmatrix}, \text{ such that } \|z_n\| \leq \sqrt{1 - (1 - \epsilon)^2}.$$

Let us define

$$\forall n \in [N - 1] : x_n = \begin{bmatrix} 1 - \epsilon \\ \sqrt{1 - (1 - \epsilon)^2} \frac{1}{\|z_n\|} z_n \end{bmatrix},$$

and $x_N = e_1$. Then, we claim $\alpha_N(\{x_n\}_{n=1}^N) \geq \alpha_N(\{y_n\}_{n=1}^N)$. Following the definition of ordinal spread, we have

$$\begin{aligned} \alpha_N(\{x_n\}_{n=1}^N) &\stackrel{(a)}{=} \text{card} \left\{ (i, j) : d(x_i, x_j) \geq d_{\max}(x_N, \{x_n\}_{n=1}^{N-1}), i, j \in [N - 1], i > j \right\} + 1, \\ &\stackrel{(b)}{=} \text{card} \left\{ (i, j) : d(x_i, x_j) \geq \text{acos}(1 - \epsilon), i, j \in [N - 1], i > j \right\} + 1, \\ &\stackrel{(c)}{\geq} \text{card} \left\{ (i, j) : d(y_i, y_j) \geq \text{acos}(1 - \epsilon), i, j \in [N - 1], i > j \right\} + 1, \\ &= \alpha_N(\{y_n\}_{n=1}^N), \end{aligned}$$

where (a) holds with equality if x_N appears last in the sorted distance list, (b) is due to $d_{\max}(x_N, \{x_n\}_{n=1}^{N-1}) = \text{acos}(1 - \epsilon) = d_{\max}(y_N, \{y_n\}_{n=1}^{N-1})$. For inequality (c), let $d(y_i, y_j) \geq \text{acos}(1 - \epsilon)$ for distinct $i, j \in [N - 1]$ and $z_i^\top z_j = \|z_i\| \|z_j\| \cos \theta_{ij}$. Therefore,

$$\begin{aligned} \cos \theta_{ij} &= \frac{1}{\|z_i\| \|z_j\|} z_i^\top z_j \\ &\stackrel{(a)}{\leq} \frac{1}{\|z_i\| \|z_j\|} \left(1 - \epsilon - \sqrt{1 - \|z_i\|^2} \sqrt{1 - \|z_j\|^2} \right) \\ &\stackrel{(b)}{\leq} 0. \end{aligned}$$

where (a) is due to

$$y_i^\top y_j = \sqrt{1 - \|z_i\|^2} \sqrt{1 - \|z_j\|^2} + z_i^\top z_j \leq 1 - \epsilon,$$

and inequality (b) is due $\sqrt{1 - \|z_i\|^2} \geq \sqrt{1 - \sqrt{1 - (1 - \epsilon)^2}^2} = \sqrt{1 - \epsilon^2}$.⁶ Then, we have

$$\begin{aligned} d(x_i, x_j) &= \text{acos} \left((1 - \epsilon)^2 + (1 - (1 - \epsilon)^2) \cos \theta_{ij} \right) \\ &\geq \text{acos} \left(\sqrt{1 - \|z_i\|^2} \sqrt{1 - \|z_j\|^2} + z_i^\top z_j \right) \\ &= d(y_i, y_j) \end{aligned}$$

since $(1 - (1 - \epsilon)^2) \cos \theta_{ij} \leq \|z_i\| \|z_j\| \cos \theta_{ij}$ where $\cos \theta_{ij} \leq 0$. Therefore, we have

$$\{(i, j) : d(y_i, y_j) \geq \text{acos}(1 - \epsilon), i, j \in [N - 1], i > j\} \subseteq \{(i, j) : d(x_i, x_j) \geq \text{acos}(1 - \epsilon), i, j \in [N - 1], i > j\}.$$

Hence, $\{x_n\}_{n=1}^N$ is an ordinally dense subset of \mathbb{S}^d . \square

Now, let us find ordinally dense set of points x_1, \dots, x_N in \mathbb{S}^d with

$$\forall n \in [N - 1] : x_n = \begin{bmatrix} 1 - \epsilon \\ z_n \end{bmatrix}, \text{ and } x_N = e_1.$$

⁵ e_1 is the first standard base vector for \mathbb{R}^{d+1} .

⁶Similarly, we have $\sqrt{1 - \|z_j\|^2} \geq \sqrt{1 - \epsilon^2}$.

We have $\|z_n\|^2 = 1 - (1 - \epsilon)^2$ for all $\forall n \in [N - 1]$. We begin from the definition of ordinal spread as follows

$$\begin{aligned}\alpha_N(\{x_n\}_{n=1}^N) &= \text{card} \left\{ (i, j) : d(x_i, x_j) \geq d_{\max}(x_N, \{x_n\}_{n=1}^{N-1}), i, j \in [N - 1], i > j \right\} + 1, \\ &= \text{card} \left\{ (i, j) : d(x_i, x_j) \geq \text{acos}(1 - \epsilon), i, j \in [N - 1], i > j \right\} + 1, \\ &= \text{card} \left\{ (i, j) : \frac{1}{\|z_i\| \|z_j\|} z_i^\top z_j \leq \frac{\epsilon(1 - \epsilon)}{1 - (1 - \epsilon)^2}, i, j \in [N - 1], i > j \right\} + 1, \\ &= \text{card} \left\{ (i, j) : \text{acos}(\widehat{z}_i^\top \widehat{z}_j) \geq \frac{\pi}{3}, i, j \in [N - 1], i > j \right\} + 1,\end{aligned}$$

where $\widehat{z}_i = \frac{1}{\|z_i\|} z_i$, $\widehat{z}_j = \frac{1}{\|z_j\|} z_j$, and $\sup_{\epsilon} \frac{\epsilon(1 - \epsilon)}{1 - (1 - \epsilon)^2} = \frac{1}{2}$. Similar to the Euclidean space, this problem is equivalent to spherical $\frac{\pi}{6}$ -cap packing number in \mathbb{R}^d , since $\widehat{z}_n \in \mathbb{R}^d$. Finally, if we assume $\min_{i, j \in [N], i > j} d(x_i, x_j) = \delta$, we have $d_{\max}(x_N, \{x_n\}_{n=1}^{N-1}) \geq \delta$. Therefore, the cap angles can be computed as follows

$$\alpha = \min_{\epsilon \geq 1 - \cos \delta} \frac{1}{2} \text{acos} \frac{\epsilon(1 - \epsilon)}{1 - (1 - \epsilon)^2} = \frac{1}{2} \text{acos} \frac{\cos \delta}{1 + \cos \delta} > \frac{\pi}{6}.$$

In this case, the ordinal capacity can be refined as spherical α -cap packing number.

6.3 Proof of Theorem 2

Let S be a d -dimensional space form, and $N \leq K(S)$. From Definition 4, we can find an ordinaly dense subset $x_1, \dots, x_N \in S$. Hence, we have

$$\begin{aligned}A_N(S) &= \sup_{x_1, \dots, x_N \in S} \alpha_N(\{x_n\}_{n=1}^N), \\ &\stackrel{(a)}{=} \binom{N - 1}{2} + 1\end{aligned}$$

where (a) directly follows from Proposition 1. This is the number of edges of a complete graph with $N - 1$ vertices plus one.

Now, let us consider $N > K(S)$. This could only happen in (d -dimensional) Euclidean and spherical spaces, since hyperbolic spaces have infinite ordinal capacity, i.e., $K(\mathbb{H}^d) = \infty$.

In Section 6.2, we proved that there is a set of points $x_1, \dots, x_{N-1} \in \mathbb{R}^d$ on the unit sphere and $x_N = 0$ such that

$$\begin{aligned}A_N(S) &= \alpha_N(\{x_n\}_{n=1}^N), \\ &= \text{card} \{(i, j) : d(x_i, x_j) \geq 1, i, j \in [N - 1], i > j\} + 1.\end{aligned}$$

Consider a pair of points $x_i, x_j \in \mathbb{R}^d$ with $d(x_i, x_j) < 1$. We can move the point x_i and place it on x_j if

$$\text{card} \{(i, k) : d(x_i, x_k) \geq 1, i, k \in [N - 1], i \neq k\} \leq \text{card} \{(j, k) : d(x_j, x_k) \geq 1, j, k \in [N - 1], j \neq k\}.$$

This condition is to ensure that we do not decrease $\alpha_N(\{x_n\}_{n=1}^N)$. We repeat this process and lump the set of $N - 1$ point on $K < N - 1$ positions, i.e., p_1, \dots, p_K . At each position p_k , we place multiple vertices. Finally, $\alpha_N(\{x_n\}_{n=1}^N)$ is equal to the number of edges – with length greater than 1 – in this K -partite graph with $N - 1$ vertices. This graph is K -partite because the distance between points in a partition have distances of zero. Hence, their edges do not contribute in calculating the ordinal spread of the point set. This graph becomes a complete K -partite graph if all distinct positions $\{p_k\}$ belong to the centers of spherical $\frac{\pi}{6}$ -caps on the unit sphere. On the other hand, the number of edges in a complete K -partite graph is maximized when the size of the parts differs by at most one, i.e., Turán graph $T(N - 1, K)$ [49]. Therefore, the N -point ordinal spread of S (Euclidean or spherical space) is given by

$$A_N(S) = \text{card } E(T(N - 1, K(S) - 1)) + 1.$$

The maximum number of possible partitions $(K(S) - 1)$ gives the maximum number of edges, i.e.,

$$\text{card } E(T(N - 1, 1)) \leq \text{card } E(T(N - 1, 2)) \leq \dots \leq \text{card } E(T(N - 1, K(S) - 1)).$$

This completes the proof.

6.4 Proof of Proposition 2

The proof follows from the definition of $A_N(S)$, the N -point ordinal spread of a space form S , in Theorem 2.

7 NUMERICAL EXPERIMENTS

All our experiments were conducted on a Dual-Core Intel Core i5 Mac machine, 16GB of system memory.

7.1 Datasets

In this paper, we used cartographic data (counties in the state of Illinois, counties in Midwestern states,⁷ and cities and towns across the world⁸) and single-cell RNA expression data⁹ [57–59, 55] which are publicly available datasets. Details of the single-cell expressions datasets are as follows:

1. *Lymphoma patient.* Human dissociated lymph node tumor cells of a 19-year-old male Hodgkin’s Lymphoma patient were obtained by 10x Genomics from Discovery Life Sciences. Whole transcriptome libraries were generated with Chromium Next GEM Single Cell 3’ Reagent Kits v3.1 (Dual Index) User Guide (CG000315) and sequenced on an Illumina NovaSeq 6000. The targeted libraries were generated using the Targeted Gene Expression Reagent Kits User Guide (CG000293) and Human Immunology Panel reagent (PN-1000246) and sequenced on an Illumina NovaSeq 6000.
2. *Lymphoma-healthy donor.* Human peripheral blood mononuclear cells (PBMCs) of a healthy female donor aged 25 were obtained by 10x Genomics from AllCells. Whole transcriptome libraries were generated with Chromium Next GEM Single Cell 3’ Reagent Kits v3.1 (Dual Index) User Guide (CG000315) and sequenced on an Illumina NovaSeq 6000. The aforementioned two datasets have 13410 samples (combined) and each for a class (binary classification). The dimension of each cell expression vector is 1020.
3. *Blood cells landmark.* We use the dataset originally from this paper and extract the gene expression data for (1) B cells, (2) Memory T cells, and (3) Native T cells. The complete dataset has 94655 samples, and the dimension of each cell expression vector is 965.
4. We use the single-cell RNA sequencing atlas provided in [55]. This atlas contains 26000 cell expression vectors for adult planarians. Each cell is a 21000-dimensional integer-valued vector representing read counts of gene expressions. Therefore, this raw data reside in a 21000-dimensional Euclidean space.

Imputations. Existing methods for denoising and imputation of raw scRNA-seq data often involve building connection graphs among cells [52, 51] using the distance between cells to diffuse the expression profiles among neighbor cells and smooth out possible outliers. In our experiment we used MAGIC [51] to impute our raw sequencing data with different number of neighbors and steps in the diffusion process to get different level of imputation results.

RFA score. For datasets (1 – 3), we construct the 5-nearest neighbor graph, and set the kernel width (σ) to have an (soft) average of 3 neighbors; see Section 2.3 for more detail on computing RFA scores.

7.2 Hyperbolicity of Trees

We generate random weighted trees with $N = 10^4$ nodes. The edge weights are drawn from i.i.d. uniform distribution in $[0, 1]$. The distance between each two nodes is the weight of the path joining them. We contaminate the corresponding distance matrix by an additive zero mean Gaussian noise with the signal to noise ratio of 40 dB. In this experiment, we consider three different trees with maximum degrees of 4, 5, 6.¹⁰ In Figure 10, we show the distribution of node degrees for each tree.

We generate random points in space forms of dimension $d = 2, \dots, 5$, from the following distributions

- Hyperbolic space: $x = [\sqrt{1 + \|z\|^2}, z^\top]^\top$, where $z \sim \mathcal{N}(0, \sigma^2 I)$ and $\sigma = 100$;
- Euclidean space: $x \sim \mathcal{N}(0, \sigma^2 I)$;
- Spherical space: $x = \frac{1}{\|z\|} z$, where $z \sim \mathcal{N}(0, I)$.¹¹

Commonly, in embedding trees, the leaves concentrate near the boundary of the Poincaré disk. Hence, we choose a large variance σ to heavily sample the points closer to the boundary of Poincaré disk. Finally, we devise a hypothesis test based on the total variation distance of probability measures,¹² i.e.,

$$\delta(P, Q) = \|P - Q\|_1.$$

For each tree T with $\Delta(T) = 4, 5$ and 6, we report the distances between the target (oracle) and empirical probability mass functions (PMF) of α_k for a set of N points generated in each space form. In Tables 1 to 3, we consider sub-cliques — randomly sampled from each tree — with $N = 20$ nodes. From the hypothesis tests for α_k , $k \in \{3, \dots, 20\}$, we conclude that the ordinal spread variables of random trees better match with hyperbolic ordinal spread variables.

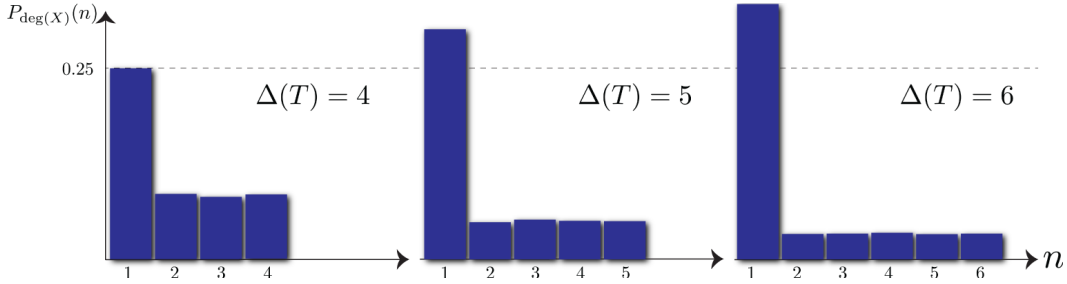


Figure 10: The distribution of node degrees for each random tree.

⁷The US Zip Code Latitude and Longitude data is available at <https://public.opendatasoft.com/explore/dataset/us-zip-code-latitude-and-longitude/>.

⁸World cities database is available at <https://simplemaps.com/data/world-cities>.

⁹We used four data sets: Lymphoma patient, healthy donor, blood cells landmark, and Planaria single cell atlas.

¹⁰In the main manuscript, we only considered a binary tree with $\Delta(T) = 3$.

¹¹Therefore, the points are distributed uniformly on \mathbb{S}^d .

¹²The total variation distance is $\delta(P, Q) = \frac{1}{2} \|P - Q\|_1$, but we can ignore the constant term.

Table 1: $\delta(P_{\alpha_k}, \hat{P}_{\alpha_k}) \times 10^{-3}$ for different space forms — $\Delta(T) = 4$.

k	3	4	5	6	7	8	9	10	11	12	13	14	15	16	17	18	19	20
\mathbb{H}^2	0	1.6	1.9	1.7	1.8	2.1	2.4	2.5	2.3	2.1	2.1	2.0	2.0	2.1	2.2	2.3	2.4	2.2
\mathbb{H}^3	0	2.3	2.8	2.5	2.4	2.5	2.9	3.0	2.9	2.6	2.5	2.3	2.2	2.0	1.9	1.8	1.8	1.7
\mathbb{H}^4	0	2.7	3.3	3.0	2.8	2.8	3.0	3.2	3.3	3.0	2.8	2.6	2.4	2.2	2.0	1.7	1.5	1.3
\mathbb{H}^5	0	3.0	3.6	3.4	3.0	3.1	3.2	3.4	3.5	3.3	3.0	2.8	2.6	2.3	2.1	1.8	1.5	1.1
\mathbb{E}^2	0	1.5	1.9	2.1	2.4	2.8	2.9	3.1	3.2	3.3	3.4	3.5	3.7	3.9	4.2	4.7	5.4	6.7
\mathbb{E}^3	0	2.2	2.7	2.6	2.8	3.4	3.5	3.7	3.7	3.8	3.9	4.0	4.1	4.1	4.3	4.5	4.9	5.9
\mathbb{E}^4	0	2.6	3.2	3.1	3.1	3.6	3.8	3.9	4.0	4.1	4.2	4.3	4.3	4.3	4.3	4.4	4.7	5.4
\mathbb{E}^5	0	2.8	3.5	3.5	3.3	3.8	3.9	4.1	4.1	4.2	4.4	4.4	4.4	4.3	4.3	4.4	4.6	5.1
\mathbb{S}^2	0	8.4	9.9	10.2	10.1	10	9.9	9.8	9.6	9.2	8.7	8.6	8.6	8.6	8.5	8.5	8.5	8.8
\mathbb{S}^3	0	8.4	9.8	10.2	10.1	10.1	10	9.9	9.6	9.3	8.8	8.7	8.7	8.7	8.7	8.7	8.7	8.8
\mathbb{S}^4	0	8.4	9.8	10.1	10.2	10.1	10	9.9	9.7	9.4	8.9	8.8	8.8	8.8	8.8	8.8	8.8	8.8
\mathbb{S}^5	0	8.5	9.8	10.1	10.2	10.1	10.1	9.9	9.7	9.4	8.9	8.9	8.9	8.9	8.8	8.8	8.8	8.7

 Table 2: $\delta(P_{\alpha_k}, \hat{P}_{\alpha_k}) \times 10^{-3}$ for different space forms — $\Delta(T) = 5$.

k	3	4	5	6	7	8	9	10	11	12	13	14	15	16	17	18	19	20
\mathbb{H}^2	0	1.6	2.0	2.6	2.8	2.8	2.8	2.6	2.6	2.5	2.4	2.2	2.1	1.9	1.7	1.4	1.1	0.7
\mathbb{H}^3	0	2.3	2.8	3.1	3.4	3.5	3.5	3.5	3.3	3.3	3.1	3.0	2.8	2.6	2.3	2.0	1.5	0.8
\mathbb{H}^4	0	2.7	3.3	3.4	3.7	3.9	3.9	3.9	3.8	3.7	3.6	3.5	3.3	3.1	2.8	2.5	2.0	1.2
\mathbb{H}^5	0	3.0	3.6	3.6	3.8	4.2	4.2	4.2	4.2	4.0	3.9	3.8	3.6	3.4	3.1	2.8	2.3	1.6
\mathbb{E}^2	0	1.5	2.3	3.4	3.6	4.0	4.2	4.4	4.6	4.8	5.0	5.3	5.6	5.9	6.3	6.9	7.5	8.4
\mathbb{E}^3	0	2.2	2.7	3.8	4.2	4.6	4.8	5.0	5.1	5.2	5.4	5.6	5.8	6.0	6.3	6.7	7.1	7.8
\mathbb{E}^4	0	2.6	3.2	3.9	4.5	4.9	5.0	5.2	5.4	5.5	5.6	5.8	5.9	6.1	6.3	6.6	6.9	7.3
\mathbb{E}^5	0	2.8	3.5	4.1	4.6	5.0	5.2	5.4	5.5	5.7	5.8	5.9	6.0	6.1	6.3	6.5	6.7	7.0
\mathbb{S}^2	0	8.4	9.9	10.2	10.1	10	9.9	9.8	9.6	9.5	9.5	9.5	9.5	9.5	9.5	9.5	9.6	9.7
\mathbb{S}^3	0	8.4	9.8	10.2	10.1	10.1	10	9.9	9.6	9.5	9.6	9.6	9.6	9.6	9.7	9.7	9.7	9.7
\mathbb{S}^4	0	8.4	9.8	10.1	10.2	10.1	10	9.9	9.7	9.6	9.6	9.7	9.7	9.7	9.7	9.8	9.8	9.7
\mathbb{S}^5	0	8.5	9.8	10.1	10.2	10.1	10.1	9.9	9.7	9.7	9.7	9.7	9.7	9.8	9.8	9.8	9.8	9.7

 Table 3: $\delta(P_{\alpha_k}, \hat{P}_{\alpha_k}) \times 10^{-3}$ for different space forms — $\Delta(T) = 6$.

k	3	4	5	6	7	8	9	10	11	12	13	14	15	16	17	18	19	20
\mathbb{H}^2	0	1.6	2.5	3.0	3.2	3.2	3.1	2.9	2.9	2.7	2.5	2.3	2.1	1.9	1.6	1.3	1.1	1.4
\mathbb{H}^3	0	2.3	2.8	3.6	3.8	3.8	3.8	3.7	3.6	3.5	3.3	3.0	2.8	2.5	2.1	1.6	1.0	0.8
\mathbb{H}^4	0	2.7	3.3	3.9	4.0	4.2	4.2	4.2	4.0	3.9	3.7	3.5	3.2	2.9	2.5	1.9	1.2	0.4
\mathbb{H}^5	0	3.0	3.6	4.0	4.2	4.5	4.5	4.4	4.3	4.1	4.0	3.8	3.5	3.2	2.8	2.2	1.5	0.5
\mathbb{E}^2	0	1.5	2.8	3.8	4.0	4.3	4.5	4.6	4.7	4.9	5.0	5.2	5.4	5.6	5.8	6.2	6.7	7.5
\mathbb{E}^3	0	2.2	3.0	4.2	4.5	4.9	5.0	5.2	5.3	5.3	5.4	5.5	5.6	5.7	5.8	6.0	6.2	6.8
\mathbb{E}^4	0	2.6	3.2	4.4	4.8	5.2	5.3	5.4	5.5	5.6	5.6	5.7	5.7	5.8	5.8	5.9	6.0	6.3
\mathbb{E}^5	0	2.8	3.5	4.5	5.0	5.3	5.4	5.6	5.7	5.7	5.8	5.8	5.8	5.8	5.8	5.8	5.8	5.9
\mathbb{S}^2	0	8.4	9.9	10.2	10.1	10	9.9	9.8	9.6	9.4	9.4	9.4	9.4	9.3	9.3	9.3	9.2	9.3
\mathbb{S}^3	0	8.4	9.8	10.2	10.1	10.1	10	9.9	9.6	9.5	9.5	9.5	9.5	9.5	9.5	9.4	9.4	9.3
\mathbb{S}^4	0	8.4	9.8	10.1	10.2	10.1	10	9.9	9.7	9.6	9.6	9.6	9.6	9.5	9.5	9.5	9.4	9.3
\mathbb{S}^5	0	8.5	9.8	10.1	10.2	10.1	10.1	9.9	9.7	9.6	9.6	9.6	9.6	9.6	9.6	9.5	9.5	9.3

Remark. Ordinal spread variables of larger sub-cliques are more effective in testing for distinguishing the curvature sign and the dimension of space forms. For instance, consider a triangle in a space form. Regardless of the presumed space form, we have

$$\alpha_k = \begin{cases} 1 & \text{if } k = 1, \\ 1 & \text{if } k = 2, \\ 2 & \text{if } k = 3, \end{cases} \quad \text{with probability 1.}$$

This is a trivial result from **Proposition 1** and the related discussion in its proof. Therefore, the statistics of α_k can not bear any useful information about the geometry of data. This fact, along with the total number of available unique sub-cliques, should be considered for implementing a proper hypothesis test based on a majority vote; see Tables 1 to 3.

Note that we can also design an aggregate hypothesis test based on α_N by defining the following distance function between P_{α_N} and \hat{P}_{α_N} , e.g., $\delta(P_{\alpha_N}, \hat{P}_{\alpha_N}) = \sum_{k=1}^N \delta(P_{\alpha_k}, \hat{P}_{\alpha_k})$. This definition involves all ordinal spread variables related to sub-cliques of size N , i.e., α_k . Then, we can perform minimum-distance hypothesis tests for sub-cliques of sizes $N \in \{5, \dots, 20\}$. For each experiment, hyperbolic spaces provide the best matches for ordinal spread variables of each random tree; see Tables 4 to 6. This aggregate hypothesis test proves to more robustly reveal the hyperbolicity of weighted trees, compared to the individual tests based on ordinal spread variable α_N .

Table 4: $\delta(P_{\alpha_N}, \hat{P}_{\alpha_N}) \times 10^{-2}$ for different space forms — $\Delta(T) = 4$.

N	5	6	7	8	9	10	11	12	13	14	15	16	17	18	19	20
\mathbb{H}^2	3.3	3.7	3.9	4.1	4.2	4.2	4.1	4.1	4.0	4.0	3.9	3.8	3.8	3.7	3.6	3.6
\mathbb{H}^3	3.0	3.8	4.2	4.6	4.7	4.7	4.7	4.6	4.6	4.5	4.4	4.4	4.3	4.2	4.1	4.0
\mathbb{H}^4	3.4	4.1	4.7	5.0	5.2	5.2	5.1	5.1	5.0	4.9	4.8	4.8	4.7	4.5	4.4	4.4
\mathbb{H}^5	3.7	4.4	5.0	5.3	5.5	5.5	5.5	5.4	5.3	5.3	5.2	5.1	5.0	4.9	4.8	4.7
\mathbb{E}^2	7.0	8.0	8.3	8.4	8.2	8.0	7.8	7.6	7.3	7.1	6.8	6.6	6.4	6.2	6.0	5.9
\mathbb{E}^3	5.9	6.9	7.9	8.1	8.0	7.9	7.9	7.8	7.6	7.5	7.3	7.1	6.9	6.7	6.6	6.4
\mathbb{E}^4	5.2	6.6	7.6	7.9	7.9	7.9	8.0	8.0	7.8	7.7	7.5	7.3	7.2	7.0	6.9	6.7
\mathbb{E}^5	5.0	6.4	7.4	7.8	7.9	8.0	8.1	8.1	8.0	7.8	7.6	7.5	7.4	7.2	7.1	6.9
\mathbb{S}^2	12.0	15.5	17.8	19.4	20.2	20.3	20.2	19.8	19.3	18.8	18.3	17.7	17.1	16.6	16.1	15.6
\mathbb{S}^3	11.8	15.5	17.8	19.5	20.2	20.4	20.3	19.9	19.5	18.9	18.4	17.9	17.3	16.8	16.2	15.7
\mathbb{S}^4	11.7	15.4	17.8	19.5	20.1	20.4	20.3	20.0	19.6	19.0	18.5	17.9	17.4	16.9	16.3	15.8
\mathbb{S}^5	11.6	15.4	17.8	19.4	20.1	20.4	20.4	20.0	19.6	19.1	18.6	18.0	17.5	16.9	16.4	15.9

Table 5: $\delta(P_{\alpha_N}, \hat{P}_{\alpha_N}) \times 10^{-2}$ for different space forms — $\Delta(T) = 5$.

N	5	6	7	8	9	10	11	12	13	14	15	16	17	18	19	20
\mathbb{H}^2	5.4	5.5	5.3	5.4	5.2	5.1	4.9	4.8	4.5	4.4	4.2	4.1	3.9	3.8	3.7	3.6
\mathbb{H}^3	4.5	4.8	5.4	5.9	5.9	5.9	5.8	5.7	5.5	5.4	5.3	5.2	5.1	4.9	4.8	4.7
\mathbb{H}^4	4.1	5.0	5.9	6.3	6.4	6.4	6.4	6.3	6.2	6.2	6.1	5.9	5.8	5.7	5.5	5.4
\mathbb{H}^5	4.2	5.2	6.2	6.6	6.8	6.8	6.8	6.8	6.8	6.7	6.6	6.4	6.3	6.2	6.1	5.9
\mathbb{E}^2	9.3	10.8	11.5	11.5	11.3	11.1	10.9	10.7	10.3	10	9.7	9.4	9.1	8.9	8.6	8.4
\mathbb{E}^3	8.0	9.6	10.6	11.0	11.0	11.1	11.0	10.8	10.5	10.3	10.0	9.7	9.5	9.3	9.0	8.8
\mathbb{E}^4	7.4	9.0	10.3	10.8	10.9	11.0	11.0	10.8	10.6	10.4	10.1	9.9	9.7	9.5	9.3	9.1
\mathbb{E}^5	6.9	8.7	10.1	10.6	10.8	10.9	10.9	10.8	10.6	10.4	10.2	10.0	9.8	9.6	9.4	9.2
\mathbb{S}^2	13.6	17.2	19.6	21.0	21.7	21.8	21.6	21.2	20.6	20.0	19.4	18.8	18.1	17.5	16.9	16.4
\mathbb{S}^3	13.4	17.3	19.8	21.1	21.8	21.9	21.8	21.3	20.8	20.2	19.6	18.9	18.3	17.7	17.1	16.5
\mathbb{S}^4	13.3	17.3	19.8	21.1	21.8	22.0	21.8	21.4	20.9	20.3	19.7	19.0	18.4	17.8	17.1	16.6
\mathbb{S}^5	13.1	17.3	19.7	21.1	21.9	22.0	21.8	21.5	20.9	20.3	19.7	19.0	18.4	17.8	17.2	16.6

Table 6: $\delta(P_{\alpha_N}, \hat{P}_{\alpha_N}) \times 10^{-2}$ for different space forms — $\Delta(T) = 6$.

N	5	6	7	8	9	10	11	12	13	14	15	16	17	18	19	20
\mathbb{H}^2	5.8	5.8	5.9	5.8	5.7	5.5	5.2	5.0	4.9	4.7	4.6	4.4	4.3	4.2	4.1	3.9
\mathbb{H}^3	4.8	5.2	5.7	5.9	6.1	6.1	5.9	5.8	5.7	5.5	5.4	5.3	5.2	5.0	4.9	4.8
\mathbb{H}^4	4.5	5.0	5.9	6.4	6.6	6.5	6.4	6.3	6.3	6.2	6.0	5.9	5.8	5.6	5.5	5.4
\mathbb{H}^5	4.3	5.1	6.2	6.7	6.9	6.9	6.8	6.7	6.7	6.6	6.5	6.3	6.2	6.1	6.0	5.8
\mathbb{E}^2	9.6	11.1	11.7	11.7	11.4	11.1	10.8	10.5	10.2	9.9	9.6	9.3	9.0	8.7	8.5	8.3
\mathbb{E}^3	8.3	9.9	10.8	11.0	10.9	10.9	10.8	10.6	10.4	10.1	9.8	9.6	9.3	9.1	8.9	8.7
\mathbb{E}^4	7.7	9.2	10.3	10.7	10.8	10.8	10.8	10.6	10.4	10.2	10.0	9.7	9.5	9.3	9.1	8.9
\mathbb{E}^5	7.2	8.8	10.0	10.5	10.6	10.8	10.8	10.6	10.4	10.2	10.0	9.8	9.6	9.4	9.2	9.0
\mathbb{S}^2	13.3	17.0	19.3	20.6	21.3	21.4	21.2	20.8	20.3	19.7	19.1	18.5	17.9	17.3	16.7	16.2
\mathbb{S}^3	13.1	17.1	19.4	20.7	21.4	21.5	21.4	20.9	20.5	19.9	19.3	18.7	18.0	17.4	16.9	16.3
\mathbb{S}^4	13.0	17.1	19.4	20.7	21.4	21.6	21.4	21.0	20.5	20.0	19.4	18.7	18.1	17.5	16.9	16.4
\mathbb{S}^5	12.9	17.1	19.4	20.7	21.4	21.6	21.5	21.1	20.6	20.0	19.4	18.8	18.2	17.6	17.0	16.4

7.2.1 On Euclidean Embedding Dimension of Trees

We generate a random tree T with $N = 10^4$ nodes, maximum degree of Δ , and i.i.d. edge weights from $\text{unif}(0, 1)$. Let $\tilde{D}_\Delta = D_\Delta + n$, where n is a zero mean Gaussian noise with 40 decibel signal-to-noise ratio, be the noisy distance matrix for T . The embedding goal is to find a representation x_1, \dots, x_N for tree nodes in S , such that

$$d(x_i, x_j) \leq d(x_k, x_l) \iff \tilde{D}_\Delta(i, j) \leq \tilde{D}_\Delta(k, l).$$

We randomly select 10^6 sub-cliques of sizes $N \in \{2, 4, \dots, 20, 100\}$. In Table 7, we give the empirical N -th ordinal spread based on non-metric measurements associated with the sub-cliques, i.e., \hat{A}_N . The distribution-free test gives a lower bound of $\hat{d} \geq 4$ for Euclidean embedding dimension.

On the other hand, consider a random weighted tree and a node x_n with degree Δ_n .¹³ We can easily see that

$$\max_{i \in [\Delta_n]} d(x_n, x_{n_i}) \leq \min_{\substack{i, j \in [\Delta_n] \\ i \neq j}} d(x_{n_i}, x_{n_j}),$$

where $x_{n_1}, \dots, x_{n_{\Delta_n}}$ are adjacent points to x_n . Hence, $\{x_n\} \cup \{x_{n_i}\}_{i=1}^{\Delta_n}$ is a set of $\Delta_n + 1$ points with maximum ordinal spread. Therefore, a lower bound for embedding dimension of a metric tree T (in Euclidean space) is given by

$$\hat{d} \geq \min \{d : K(\mathbb{R}^d) \geq \Delta(T) + 1\}$$

The exponential growth of ρ_d gives $\hat{d} = \Omega(\log \Delta(T))$.

Remark. In absence of any prior information for proper distributions of data points, the estimate for the dimension of underlying space form is unreliable. The statistics of the ordinal spread variables are *invariant* with respect isotonic transformation of data points, e.g., rotation, translation, and uniform scaling in Euclidean space.

 Table 7: The N -point ordinal spread for $\mathbb{E}^2, \mathbb{E}^3, \mathbb{E}^4$ versus \hat{A}_N estimated from \tilde{D}_4, \tilde{D}_5 and \tilde{D}_6 .

N	6	8	10	12	14	16	18	20	100
$\tilde{D}_4 : \hat{A}_N$	11	22	37	56	79	106	137	169	4421
$\tilde{D}_5 : \hat{A}_N$	11	22	37	56	79	106	136	172	4412
$\tilde{D}_6 : \hat{A}_N$	11	22	37	56	79	106	137	170	4454
$A_M(\mathbb{E}^2)$	11	21	34	51	71	94	121	151	4048
$A_N(\mathbb{E}^3)$	11	22	37	56	79	106	135	168	4573
$A_N(\mathbb{E}^4)$	11	22	37	56	79	106	137	172	4741

¹³We assume the existence of a perfect embedding.

Fact 1. Let $\{x_n\}_{n=1}^N$ be a set of points in (S, d) . The ordinal spread vector is invariant with respect to strongly isotonic transformation [39] of points. In other words, let $\psi : S \rightarrow S$ be an arbitrary function such that for all $x, y, z, w \in S$ we have

$$\begin{aligned} d(x, y) < d(z, w) &\Rightarrow d(\psi(x), \psi(y)) < d(\psi(z), \psi(w)), \\ d(x, y) = d(z, w) &\Rightarrow d(\psi(x), \psi(y)) = d(\psi(z), \psi(w)), \end{aligned}$$

then, $\alpha(\{x_n\}_{n=1}^N) = \alpha(\{\psi(x_n)\}_{n=1}^N)$.

Therefore, we can also use compact distributions, e.g., the multivariate uniform distribution. The arbitrary choices of Gaussian and uniform distributions do not significantly change the statistics of the ordinal spread variables — at least, it does not affect the key results in this experiment.

7.3 Single-cell RNA Expression Data

We use the single-cell RNA sequencing atlas provided in [55]. This atlas contains 26000 cell expression vectors for adult planarians. Each cell is an integer-valued vector representing read counts of gene expressions. The specific choices of pre-processing method and the comparison criteria *imply* a geometry — namely, geometry of similarity comparisons — that is not necessarily related to the domain of data vectors. The choice of comparisons are as follows:

- **ℓ_2 distance:** The points x_i, x_j are more similar to each other than x_k, x_l if $\|x_i - x_j\|_2 \leq \|x_k - x_l\|_2$. The *true* geometry of comparisons is a 21000-dimensional Euclidean space;
- **Angles:** The points x_i, x_j are more similar than x_k, x_l if $\angle(x_i, x_j) \leq \angle(x_k, x_l)$, where

$$\angle(x_i, x_j) \stackrel{\text{def}}{=} \arccos \frac{(x_i - \mu)^\top (x_j - \mu)}{\|x_i - \mu\| \|x_j - \mu\|},$$

and $\mu = \frac{1}{N} \sum_{n \in [N]} x_n$. We use spherical distance to compare cell vectors. The geometry of comparisons is a spherical space of dimension $21000 - 1$.

- **Relative forest accessibility (RFA) index:** For a set of points x_1, \dots, x_N , we construct the local connectivity edge set E from a symmetric k -nearest neighbor method. The relative forest accessibility matrix is a $N \times N$ doubly stochastic matrix defined as $P = (I + L)^{-1}$ where $L = D - A$ is the Laplacian matrix, $A = (A_{i,j})$ such that

$$A_{i,j} = \exp\left(-\frac{\|x_i - x_j\|^2}{2\sigma^2}\right) [(i, j) \in E],$$

where the Iverson bracket $[(i, j) \in E] = 1$ if $(i, j) \in E$ and is 0 otherwise, and D is a diagonal matrix with $D_{ii} = \sum_{j \in [N]} A_{i,j}$. The ij -th element of P is the probability of a spanning forest includes a rooted tree at x_i and is connected to x_j — a measure of similarity between x_i and x_j [18]. In this experiment, we let $\sigma = \frac{1}{\sqrt{10N^2}} \sum_{i,j \in [N]} \|x_i - x_j\|$ and ignore the hard edge assignment since the conservative choice of kernel width performs a soft edge assignment; see Figure 11 (b). For a fast implementation of $P = (I + L)^{-1}$, we approximate the weighted adjacency matrix $A \in \mathbb{R}^{N \times N}$ with a rank-500 semidefinite matrix — via a simple eigenvalue thresholding — and use Woodbury matrix identity to compute P . The points x_i, x_j are more similar than x_k, x_l if the relative forest accessibility index $p_{i,j}$ is greater than $p_{k,l}$. The geometry of RFA comparisons is unknown.

We propose heavy-tailed distributions for oracle distributions. To confirm the validity of this choice, we generate random normal, and log-normal (a heavy-tailed distribution) of various dimensions $d = 2, \dots, 20$, and different scale parameters; see Figure 11 (a). The log-normal distributions gives a better match for the empirical distribution of $\|X - \mathbb{E}X\|$ — which we denote as a *side information*. Specifically, we generate points according to the following distributions to find the optimal dimension and scale parameter a :

- Hyperbolic space: $x = [\sqrt{1 + \|z\|^2}, z^\top]^\top$, where $z \sim e^{a\mathcal{N}(0, I)} - \mathbb{E}e^{a\mathcal{N}(0, I)}$;
- Euclidean space: $x \sim e^{a\mathcal{N}(0, I)}$;

- Spherical space: $x = \frac{1}{\|z\|}z$, where $z \sim e^{a\mathcal{N}(0,I)} - \mathbb{E}e^{a\mathcal{N}(0,I)}$.

Therefore, we approximate the distribution of RNAseq read counts by (projected) log-normal distributions in a space form. In bioinformatics, the heavy-tailed distribution of gene expression reads is a well-known fact [60].

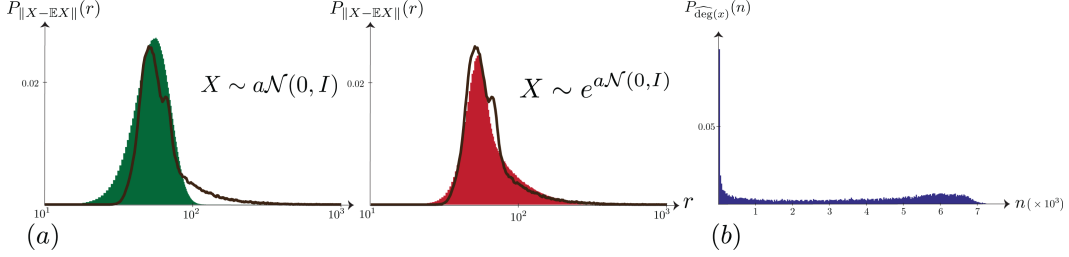


Figure 11: (a) Left: The empirical distribution of the norm of centered cell vectors (brown), and distribution of the norm of Gaussian points (green) for $d = 8$, and $a = 21.5$; (a) Right: The distribution of the norm of centered log normal points (red) for $d = 7$ and $a = 20$. (b): The distribution of *soft* degrees of each node, i.e., $\widehat{\deg}(x_n) = \sum_{m \in [N]} A_{nm}$.

ℓ_2 distances: Let $d \in \{2, 10, 10^2, 10^3, 10^4\}$, and sub-cliques of size $N = 20$. For a space form of dimension d , we iterate over a set of scale parameters a , and pick the point distribution P_X that produces the closest ordinal spread distribution to the empirical distribution of α_{20} . We show that our proposed test detects the Euclidean space of dimension 100 as the geometry of ℓ_2 comparisons. However, higher dimensional Euclidean spaces could also be plausible choices; see Figure 12.

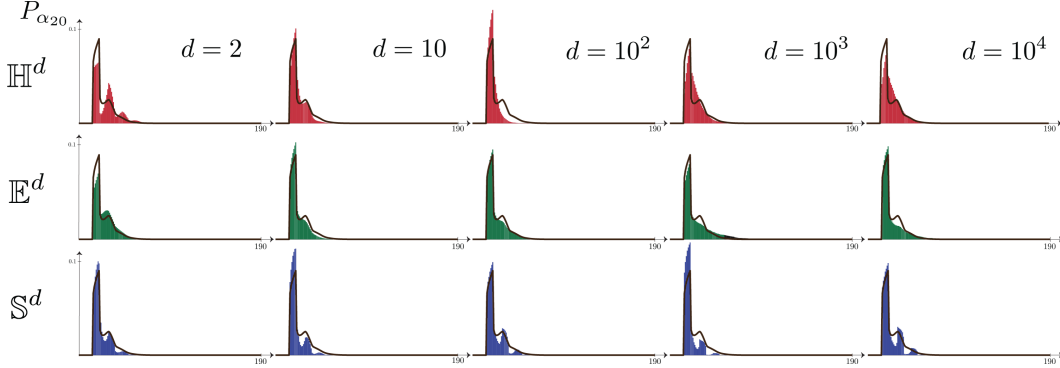


Figure 12: Brown curves represent the empirical PMF of α_{20} derived from ℓ_2 comparisons. In each row, we generate points from the corresponding space form of dimension d . This test reveals a high-dimensional Euclidean space for the geometry of ℓ_2 comparisons ($d^* = 100$).

Angular distance: We repeat the experiment for angle comparisons explained earlier. Our proposed test identifies 10000-dimensional spherical space as the geometry of angle comparisons; see Figure 13.

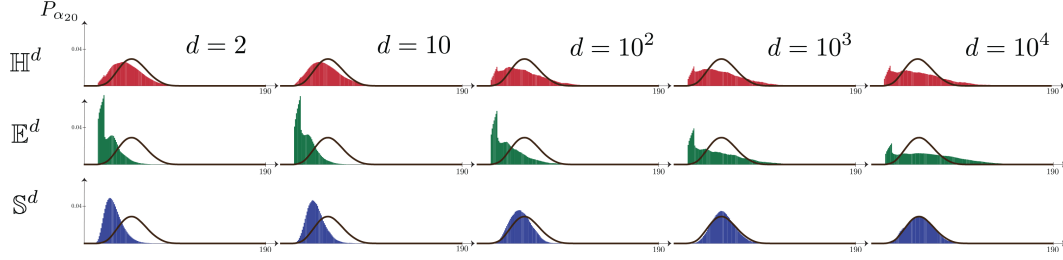


Figure 13: Brown curves represent the empirical PMF of α_{20} from angle comparisons. In each row, we generate points from the corresponding space form of dimension d . This test reveals a high-dimensional spherical space for the geometry of angle comparisons ($d^* = 10000$).

RFA index comparisons: This test identifies 1000-dimensional spherical space as the geometry of RFA index comparisons; see Figure 14. For embedding ordinal measurements, we pick a random clique of size 200 and embed it in low-dimensional space forms of different dimensions. Then, we compute the empirical probability of erroneous comparison, i.e., error occurs if $d(x_i, x_j) \geq d(x_k, x_l)$ whereas the points x_i, x_j are more similar to each other compared to the points x_k, x_l . We repeat the experiment 200 times, and report the mean and standard deviations of the probability of error p_e . An important observation is that higher dimensional of space forms do not necessarily give better matches for the empirical PMF of ordinal spread variables.

8 EMBEDDING ALGORITHMS

We can use semidefinite programs to solve non-metric embedding problems in hyperbolic and Euclidean spaces [25, 16]. The main objects in these problems are distance matrices, and the matrix of inner products, e.g., Gramian in Euclidean space and Lorentzian matrix in hyperbolic space. The traditional interior point method to solve semidefinite programs do not scale to large problems. This is especially the case for non-metric embedding problems in which we have $\binom{N}{2} = O(N^2)$ distinct inequality constraints related to pairwise distance comparisons. Therefore, we propose non-metric embedding algorithms based on the method of alternative projections; see Algorithms 1 to 3.

8.1 Hyperbolic Embedding

We start with an arbitrary hyperbolic distance matrix (refer to [25]), and a sorted index list. The function `IndexList(D)` computes the index list associated with the distance matrix D .

We begin with arranging the elements of D according to the target index list (i, j) . In other words, we have

$$\text{sort}(D, (i, j)) = (d_{\pi(i_r, j_r)})_{i_r, j_r \in [N]}$$

where $\pi : [N]^2 \rightarrow [N]^2$ is a one-to-one map, such that $\pi(i_r, j_r) = \pi(j_r, i_r)$, $\pi(i_r, i_r) = (i_r, i_r)$, and $\text{IndexList}(\text{sort}(D, (i, j))) = (i, j)$. The resulting symmetric matrix is no longer a valid hyperbolic distance matrix. Therefore, we proceed with finding the best rank- $(d + 1)$ Lorentzian matrix—the matrix of Lorentzian inner products. We compute the corresponding point set, in \mathbb{R}^{d+1} ,

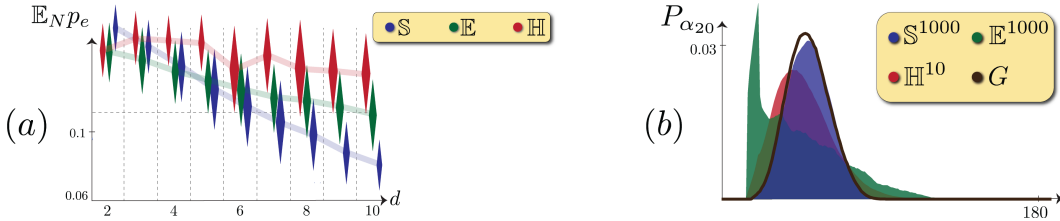


Figure 14: (a) PMFs of α_{20} from the RFA similarity graph (G) vs. random points in space forms of optimal dimensions. (b) $\mathbb{E}_N p_e$ for embedded points in d -dimensional space forms.

by a simple spectral factorization of the Lorentzian matrix; see Algorithm 1 lines 6 – 8 and refer to [25]. Finally, we use a simple method to map each point (columns of X) to \mathbb{L}^d , viz.,

$$P_{\mathbb{R}^{d+1} \rightarrow \mathbb{L}^d}(x) = \begin{bmatrix} \sqrt{1 + \|y\|^2} \\ y \end{bmatrix} \text{ where } y = (x_2, \dots, x_{d+1})^\top.$$

We compute the hyperbolic Gramian, $G = X^\top H X$, where $H = \text{diag}(-1, 1, \dots, 1) \in \mathbb{R}^{(d+1) \times (d+1)}$. This gives us the update for hyperbolic distance matrix $D = \text{acosh}[-G]$; refer to [25]. We repeat this process till convergence.

Algorithm 1 Non-metric hyperbolic embedding

```

1: procedure HYPERBOLICEMBEDDING( $(i, j), d$ )
2:   input: Index list  $(i, j)$ , and embedding dimension  $d$ .
3:   initialize: hyperbolic distance matrix  $D$ , and an arbitrary index list  $(\tilde{i}, \tilde{j})$ .
4:   while  $\|(\tilde{i}, \tilde{j}) - \text{IndexList}(D)\| > 0$  do
5:      $(\tilde{i}, \tilde{j}) \leftarrow \text{IndexList}(D)$ . ▷ The index list related to  $D$ .
6:      $D \leftarrow \text{sort}(D, (i, j))$ . ▷ Update  $D$  by sort distances according to  $(i, j)$ .
7:     Let  $U \Sigma U^\top$  be the eigenvalue decomposition of  $G = -\cosh[D]$  such that  $\sigma_1 \geq \dots \geq \sigma_N \in \mathbb{R}$ .
8:      $X = |\Sigma_d|^{1/2} U_d^\top$ , where  $\Sigma_d = \text{diag}[(\sigma_1)_+, \dots, (\sigma_d)_+, (\sigma_N)_-]$  and  $U_d$  is the sliced eigenvector matrix.
9:      $X \leftarrow P_{\mathbb{R}^{d+1} \rightarrow \mathbb{L}^d}(X)$ . ▷ Map each column of  $X \in \mathbb{R}^{(d+1) \times N}$  to  $\mathbb{L}^d$ .
10:     $G = X^\top H X$ . ▷ Hyperbolic Gramian.
11:     $D \leftarrow \text{acosh}[-G]$ . ▷ Hyperbolic distance matrix.
12:   end while
13:   return  $X$ 
14: end procedure

```

8.2 Spherical Embedding

We propose a similar method for spherical embedding. The matrix of inner products G and the spherical distance matrix D are related via $D = \text{acos}[G]$. For points in d -dimensional spherical space, the matrix G is a positive semidefinite matrix of rank $(d + 1)$, and with diagonal elements of 1. The spectral factorization of G gives us the point positions.

At each iteration of Algorithm 2, we shuffle the elements of the distance matrix according to the target index list, but the corresponding Gram matrix $G = \cos[\text{sort}(D, (i, j))]$ is not a valid Gram matrix for points in \mathbb{S}^d . We first find the best rank- $(d + 1)$ positive semidefinite matrix via a simple eigenvalue thresholding which gives a set of points in \mathbb{R}^{d+1} — as opposed to \mathbb{S}^d ; see line 9 of Algorithm 2. Therefore, we radially project each point to \mathbb{S}^d , i.e., $P_{\mathbb{R}^{d+1} \rightarrow \mathbb{S}^d}(x) = \frac{1}{\|x\|} x$. We repeat this process till a convergence is achieved.

Algorithm 2 Non-metric spherical Embedding

```
1: procedure SPHERICALEMBEDDING( $(i, j), d$ )
2:   input: Index list  $(i, j)$ , and embedding dimension  $d$ .
3:   initialize: Spherical distance matrix  $D$ , and an arbitrary index list  $(\tilde{i}, \tilde{j})$ .
4:   while  $\|(\tilde{i}, \tilde{j}) - \text{IndexList}(D)\| > 0$  do
5:      $(\tilde{i}, \tilde{j}) \leftarrow \text{IndexList}(D)$ . ▷ The index list related to  $D$ .
6:      $D \leftarrow \text{sort}(D, (i, j))$ . ▷ Update  $D$  by sort distances according to  $(i, j)$ .
7:     Let  $U\Sigma U^\top$  be eigenvalue decomposition of  $G = \cos[D]$  such that  $\sigma_1 \geq \dots \geq \sigma_N \in \mathbb{R}$ .
8:     Let  $\Sigma_d = \text{diag}[(\sigma_1)_+, \dots, (\sigma_{d+1})_+]$ , and  $U_d$  be corresponding eigenvector matrix.
9:      $X = \Sigma_d^{1/2} U_d^\top$ .
10:     $X \leftarrow P_{\mathbb{R}^{d+1} \rightarrow \mathbb{S}^d}(X)$ . ▷ Map each column of  $X \in \mathbb{R}^{(d+1) \times N}$  to  $\mathbb{S}^d$ .
11:     $G = X^\top X$ . ▷ The Gram matrix.
12:     $D \leftarrow \text{acos}[G]$ .
13:   end while
14:   return  $X$ 
15: end procedure
```

8.3 Euclidean Embedding

Unlike hyperbolic and spherical counterparts, Euclidean distance matrix $D \in \mathbb{R}^{N \times N}$ is the matrix of squared distances between a set of N points $X \in \mathbb{R}^{d \times N}$. This definition lets us to express it as a linear function of the Gram matrix $G = X^\top X$, i.e., $D = \mathcal{K}(G) = -2G + \text{diag}(G)1^\top + 1\text{diag}(G)^\top$, where $\text{diag}(G)$ is a vector of diagonal elements of G , and $1 \in \mathbb{R}^N$ is the vector of all ones. The Gram matrix G is positive semidefinite of rank at most d . We can find the centered Gramian from a given distance matrix as $G = -\frac{1}{2}JDJ$, where $J = I - \frac{1}{N}11^\top$. At each iteration of Algorithm 3, we find the best rank- d positive semidefinite matrix via a simple eigenvalue thresholding of $G = -\frac{1}{2}JDJ$; see lines 7 – 8 of Algorithm 3. The spectral factorization of G gives the point set in \mathbb{R}^d . We repeat this process until convergence.

Algorithm 3 Non-metric Euclidean embedding

```
1: procedure EUCLIDEANEMBEDDING( $(i, j), d$ )
2:   input: Index list  $(i, j)$ , and embedding dimension  $d$ .
3:   initialize: hyperbolic distance matrix  $D$ , and an arbitrary index list  $(\tilde{i}, \tilde{j})$ .
4:   while  $\|(\tilde{i}, \tilde{j}) - \text{IndexList}(D)\| > 0$  do
5:      $(\tilde{i}, \tilde{j}) \leftarrow \text{IndexList}(D)$ . ▷ The index list related to  $D$ .
6:      $D = \text{sort}(D, (i, j))$ .
7:     Let  $U\Sigma U^\top$  be the eigenvalue decomposition of  $G = -\frac{1}{2}JDJ$  such that  $\sigma_1 \geq \dots \geq \sigma_N \in \mathbb{R}$ .
8:      $G = U_d \Sigma_d U_d^\top$ , where  $\Sigma_d = \text{diag}[(\sigma_1)_+, \dots, (\sigma_d)_+]$  and  $U_d$  is the sliced eigenvector matrix.
9:      $D \leftarrow \mathcal{K}(G)$ . ▷ Euclidean distance matrix.
10:   end while
11:   return  $X = \Sigma_d^{1/2} U_d^\top$ .
12: end procedure
```
